

Combination and Reinterpretation of LHC SUSY Searches

Alexander Feike^a, Juri Fiaschi^{b,c}, Benjamin Fuks^d, Michael Klasen^a and Alexander Puck Neuwirth^a

^a*Institut für Theoretische Physik, Universität Münster, Wilhelm-Klemm-Straße 9, 48149 Münster, Germany*

^b*Università degli Studi di Milano-Bicocca, Department of Physics “Giuseppe Occhialini”, & INFN, Sezione di Milano-Bicocca, Piazza della Scienza 3, Milano 20126, Italy*

^c*Department of Mathematical Sciences, University of Liverpool, Liverpool L69 3BX, United Kingdom*

^d*Laboratoire de Physique Théorique et Hautes Énergies (LPTHE), UMR 7589, Sorbonne Université et CNRS, 4 place Jussieu, 75252 Paris Cedex 05, France*

E-mail: alex.feike@uni-muenster.de, juri.fiaschi@unimib.it,
fuks@lpthe.jussieu.fr, michael.klasen@uni-muenster.de,
alexander.neuwirth@uni-muenster.de

ABSTRACT: To maximise the information obtained from various independent new physics searches conducted at the LHC, it is imperative to consider the combination of multiple analyses. To showcase the exclusion power gained by combining signal regions from different searches, we consider a simplified scenario inspired by supersymmetry, with all particles but one squark flavour and a bino-like neutralino decoupled. The corresponding signal therefore comprises strong squark pair production, associated squark-neutralino production, as well as weak neutralino pair production. We find that considering the associated and strong production mechanisms together significantly impacts mass limits, while contributions from the weak production are insignificant in the context of current exclusion limits. In addition, we demonstrate that the combination of uncorrelated signal regions as assessed from the recent TACO approach substantially pushes exclusion limits towards higher masses, relative to the bounds derived from the most sensitive individual analyses.

Contents

1	Introduction	1
2	Theoretical setup and hard-scattering signal simulation	3
3	Analysis setup	5
3.1	Recast of single experimental analyses	7
3.2	Combining the analyses	8
4	Results	10
5	Conclusion	14
A	Event generation and multi-partonic matrix element merging	15
B	Statistical analysis	18
C	Tables	21

1 Introduction

Observations like the rotation curves of remote stars or gravitational lensing strongly indicate that our Universe includes more than just visible matter and the neutrinos of the Standard Model (SM). A promising idea to explain this surplus of mass is to introduce a stable, or at least long living, weakly interacting massive particle (WIMP) in a Beyond the Standard Model (BSM) theory. One appealing possibility for such a construction is to extend the theory symmetry group with fermionic operators. This leads to the concept of supersymmetric (SUSY) quantum field theories, which additionally maximally extend the Poincaré group [1–3]. To comply with dark matter considerations, most SUSY models, and in particular the minimal supersymmetric realisation called the Minimal Supersymmetric Standard Model (MSSM), further assume the conservation of a multiplicative quantum number dubbed R -parity [4]. This results in phenomenologically viable SUSY spectra where the lightest supersymmetric particle (LSP) is electrically neutral [5].

Consequently, intensive searches for SUSY particles have been taken up at high-energy particle colliders like the Large Hadron Collider (LHC) at CERN. The ATLAS and CMS experiments at the LHC initially focused on signatures of the strong production of squarks and gluinos [6, 7], and next extended their searches to incorporate weak production channels, *i.e.* the pair production of neutralinos, charginos and sleptons [8–11]. Although no evidence for SUSY has been found yet, it remains a cutting-edge research topic until today. Recent experimental analyses at the LHC [12–16] pushed the lower bounds on the SUSY masses

deep into the TeV regime, the exact limit depending on the scenario considered. However, in certain model scenarios such as when the SUSY spectrum is compressed, these limits may not apply, allowing for potential escape routes from the constraints imposed experimentally. While limits are usually cast in the context of simplified models inspired by the MSSM and in which only a few SUSY states are light, data can be reinterpreted in different, non-minimal and more realistic, scenarios. In this case, typical SUSY signals often comprise several components. For instance, in the framework of a scenario featuring light squarks and a neutralino LSP, a SUSY signature made of jets and missing transverse energy could arise from both squark-pair and associated squark-neutralino production, in contrast with simplified model setups in which only a single production channel is considered. The mutual impact of these two processes on SUSY exclusions computed from the signal region of a specific LHC analysis providing the best expectation has been recently examined [17]. Light was shed on the existence of a non-trivial improvement on the SUSY bounds, which finds its origin in a more accurate modelling of the *full* SUSY signal by incorporating all its potentially relevant components.

To further profit from the already collected data and from all searches for multiple jets and missing energy, it is necessary to also add pure weak production channels in which a pair of electroweakinos is produced. Such weak processes could indeed be relevant in specific regions of the SUSY parameter space. Furthermore, the new physics search programme at the LHC includes a variety of searches for jets and missing transverse energy, each leveraging slightly different handles on the signal. It is therefore crucial to combine signal regions (SRs) of any specific analysis as well as different analyses, although this must be achieved in a statistically sound approach without double counting any effect. Experimental collaborations have recently made efforts to provide information on the statistical models used for limit setting, including correlations between SRs, either exactly [18] or approximately [19]. However, comprehensive information is only available for a limited number of LHC analyses. On the other hand, the code **TACO** [20] tackles the problem of combining SRs from different channels in an approximate manner, by determining the existing correlation between SRs of possibly different LHC analyses for a specific set of signal events. This information then provides a way to compute exclusion limits from the best possible and meaningful combination of a given set of SRs, that is in practice obtained by means of a graph-based algorithm. While this approach offers a first insight into the gain in sensitivity achieved by combining SRs from various analyses, it ignores correlated systematic uncertainties like those originating from parton densities, luminosity measurements or limitations arising from overlapping signal regions of a particular analysis and control regions from other analyses.

In this work, we calculate the best estimation to date of limits on non-minimal SUSY models with squarks and electroweakinos, complementing earlier work assessing the gain in sensitivity obtained from the combination of various ATLAS and CMS searches for electroweakinos [21] and third-generation squarks [22]. These bounds are obtained not only from simulations of the full corresponding SUSY signal, but also from the combination of several searches for SUSY relying on jets and missing transverse energy. To this aim, we consider a simplified SUSY scenario in which the set of relevant superpartners is restricted to one neutralino and one squark, as described in Section 2. In this section, we also discuss

the different processes contributing to the signal. Limits are determined from the toolchain setup introduced in Section 3, that allows for event generation, detector simulation, cross section calculation, LHC recasting and SR combination. The results displayed in Section 4 then showcase the resulting gain in exclusion power. Finally, we conclude in Section 5.

2 Theoretical setup and hard-scattering signal simulation

We consider a simplified model inspired by the MSSM, in which the SM is extended by one squark flavour $\tilde{q} \equiv \tilde{u}_R$ and one neutralino state $\tilde{\chi}_1^0$, all other superpartners having masses of 30 TeV and being thus decoupled. Furthermore, the neutralino mixing matrix is taken to be diagonal, so that the lightest $\tilde{\chi}_1^0$ state is effectively bino-like. In this new physics parametrisation, the mass of the squark $m_{\tilde{q}}$ and that of the neutralino $m_{\tilde{\chi}_1^0}$ are free parameters, and their values are imposed to satisfy the condition $m_{\tilde{q}} > m_{\tilde{\chi}_1^0}$. This ensures that the $\tilde{\chi}_1^0$ state is the LSP, and therefore a good candidate for dark matter (thanks to R -parity conservation). The associated collider signal therefore includes three processes: the strong production of a pair of squarks ($pp \rightarrow \tilde{q}\tilde{q}^*$), the associated production of a neutralino and a squark ($pp \rightarrow \tilde{q}\tilde{\chi}_1^0 + \text{H.c.}$), and the weak production of a pair of neutralinos ($pp \rightarrow \tilde{\chi}_1^0\tilde{\chi}_1^0$). All superpartners different from the \tilde{q} and $\tilde{\chi}_1^0$ states being decoupled, the squark \tilde{q} is unstable and always decays promptly via the process $\tilde{q} \rightarrow \tilde{\chi}_1^0 q$. The global signature of the signal, once squark decays are accounted for, is therefore made of multiple jets and missing transverse energy carried away by the stable neutralino states.

In this way, signal simulation is achieved by means of `MadGraph5_aMC@NLO 3.5.1` [23]. Making use of the UFO [24] implementation of the MSSM [25] obtained with `FeynRules` [26, 27], we independently generate hard-scattering events for the three considered sub-processes. To this aim, we convolute leading-order (LO) matrix elements featuring up to two additional jets (from either initial-state or final-state radiation) with the `MSHT201o_as130` [28] LO set of parton distribution functions (PDFs) provided by `LHAPDF 6.5.4` [29]. To maintain consistency in the analysis, it is imperative to avoid double counting any contribution across the three production modes. Thus, we manually prohibit intermediate squarks from being on-shell in any $2 \rightarrow 3$ or $2 \rightarrow 4$ diagram (*i.e.* with one or two QCD emissions). The produced events are next re-weighted according to K -factors defined by the ratio of total rates including state-of-the-art higher-order corrections obtained with `Resummino 3.1.2` [30] and `NNLL-fast 2.0` [31] to LO predictions computed with these two codes.

Neutralino pair production cross sections are calculated with `Resummino`.¹ The code combines, following the standard threshold resummation formalism [33–35], matrix elements including approximate next-to-next-to-leading-order (aNNLO) corrections in QCD [36, 37] with the resummation of soft-gluon radiation at the next-to-next-to-leading-logarithmic (NNLL) accuracy [37–40]. We additionally use `Resummino` to compute associated neutralino-squark production rates by matching next-to-leading-order (NLO) matrix elements [41] with threshold resummation at the next-to-leading-logarithmic (NLL) accuracy [42]. Finally, total cross sections for squark pair production are calculated with `NNLL-fast`. The latter

¹Executed via the Python interface `HEPi` [32].

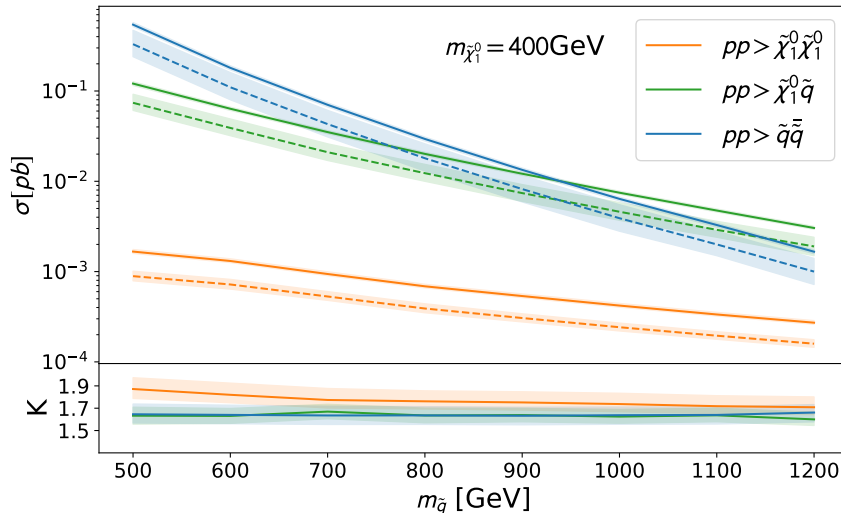


Figure 1: Leading-order (dashed) and higher-order resummed (solid) cross section predictions in pp collisions at the LHC with a centre-of-mass energy of 13 TeV for the three considered processes (upper panel) and associated K -factors (lower panel) including scale uncertainties, for a scenario featuring a fixed neutralino mass of $m_{\tilde{\chi}_1^0} = 400$ GeV and a varying squark mass $m_{\tilde{q}}$.

combines aNNLO matrix elements [43, 44], soft-gluon resummation at NNLL in the absolute threshold limit, and the resummation of Coulomb gluons with an NLO Coulomb potential and bound-state contributions [45–50].²

As an illustration of the impact of the K -factors for the three processes considered, we focus on a scenario in which the mass of the lightest neutralino is fixed to $m_{\tilde{\chi}_1^0} = 400$ GeV, and we then show in Fig. 1 the dependence of the three production cross sections on the squark mass $m_{\tilde{q}}$. We present, in the upper panel of the figure, predictions at LO (dashed lines) and after including state-of-the-art higher-order corrections in QCD (solid lines). As expected, the relative uncertainties stemming from scale variation, that are also shown on the figure, decrease significantly when adding resummation contributions to the LO cross sections. We remind that a thorough error handling including PDF uncertainties for resummed cross sections can be found in [30, 42] for the weak and associated production channels. In the following analysis, the experimental errors nevertheless dominate such that the theoretical uncertainties are only shown to present an overview. In the lower inset of the figure, we additionally display the ratio between the two. For light squarks, the cross section corresponding to strong squark pair production ($\sigma \propto \alpha_S^2$) is the highest, while the semi-weak/semi-strong associated neutralino-squark production cross section ($\sigma \propto \alpha_S \alpha$) and the weak neutralino pair production cross section ($\sigma \propto \alpha^2$) are suppressed by about

²While NNLL-*fast* assumes a tenfold-degenerate squark spectrum, the dependence of the cross section on the nature of the squarks factorises when the gluino is decoupled. Moreover, NNLL-*fast* is unable to calculate rates at precision below NLO. We therefore utilise its predecessor NLL-*fast* [51] and its predictions at NLO and LO to calculate a global K factor defined by $K = (\sigma_{\text{NLO}}/\sigma_{\text{LO}})_{\text{NLL-}i\text{fast}} \times (\sigma_{\text{aNNLO+NNLL}}/\sigma_{\text{NLO}})_{\text{NNLL-}i\text{fast}}$.

one and three orders of magnitude, respectively. As the squark gets heavier, the strong cross section decreases quickly due to phase space suppression, and is eventually overcome by the semi-weak process rates. The turnover occurs, in our example with $m_{\tilde{\chi}_1^0} = 400$ GeV, at around $m_{\tilde{q}} \approx 920$ GeV. By virtue of the same effect, at even higher squark masses the purely weak process become increasingly relevant. K -factors are generally large and exhibit little dependence on the squark mass. Such large K -factors (especially for small squark masses in the weak $pp \rightarrow \tilde{\chi}_1^0 \tilde{\chi}_1^0$ channel) have been cross-checked with `Prospino` [52], and are also outlined in [53].

Taking into account current exclusions that slowly reach the TeV regime, all three processes could have comparable cross sections in any given realistic scenario. Their contribution in the modelling of the SUSY signal should therefore be correctly incorporated, which further motivates the necessity of their unified analysis as achieved in this study.

3 Analysis setup

The computation of the exclusion associated with each point in the model parameter space follows the toolchain outlined in Fig. 2. For every combination of squark and neutralino masses, we generate 150 k events with `MadGraph5_aMC@NLO 3.5.1 (MG5aMC)` which is then interfaced with `Pythia 8.306` [54] for parton showering and hadronisation. Furthermore, we utilise `Pythia` to merge event samples featuring a different final-state partonic multiplicity following the CKKW-L algorithm [55–57], with a merging scale set to one quarter of the SUSY hard scale defined by the average mass of the produced heavy particles. This scale is thus equal, for the three considered sub-processes, to

$$Q_{\text{MS}} = \begin{cases} \frac{1}{4}m_{\tilde{\chi}_1^0} & \text{for } pp \rightarrow \tilde{\chi}_1^0 \tilde{\chi}_1^0 \\ \frac{1}{8}(m_{\tilde{q}} + m_{\tilde{\chi}_1^0}) & \text{for } pp \rightarrow \tilde{\chi}_1^0 \tilde{q} + \tilde{\chi}_1^0 \tilde{q}^* \\ \frac{1}{4}m_{\tilde{q}} & \text{for } pp \rightarrow \tilde{q} \tilde{q}^* \end{cases} . \quad (3.1)$$

We refer to Appendix A for additional details on the merging procedure. The event weights are then re-scaled so that total rates encompass higher-order resummed corrections, as described in Section 2.

We simulate the response of the LHC detectors using `MadAnalysis5 1.10.2 (MA5)` [58–60], which relies either on `Delphes 3` [61] or its built-in `SFS` simulator [62]. For each LHC analysis considered (detailed in Section 3.1), we employ a tuned detector parametrisation and the validated analysis implementation within `MA5`. This allows us to assess the selection efficiency for our signal across all SRs of all analyses examined, and to construct an acceptance matrix where each event corresponds to a row and each SR to a column. We next utilise the software `TACO` [20] to convert the acceptance matrix into a correlation matrix. This conversion enables the determination of which combination of uncorrelated SRs yields the highest exclusion power. To achieve this, we employ a generalised version of the `PathFinder` software, initially implemented within `TACO`.³ The obtained information is

³This generalised version of the `PathFinder` software can be found at <https://github.com/J-Yellen/PathFinder>.

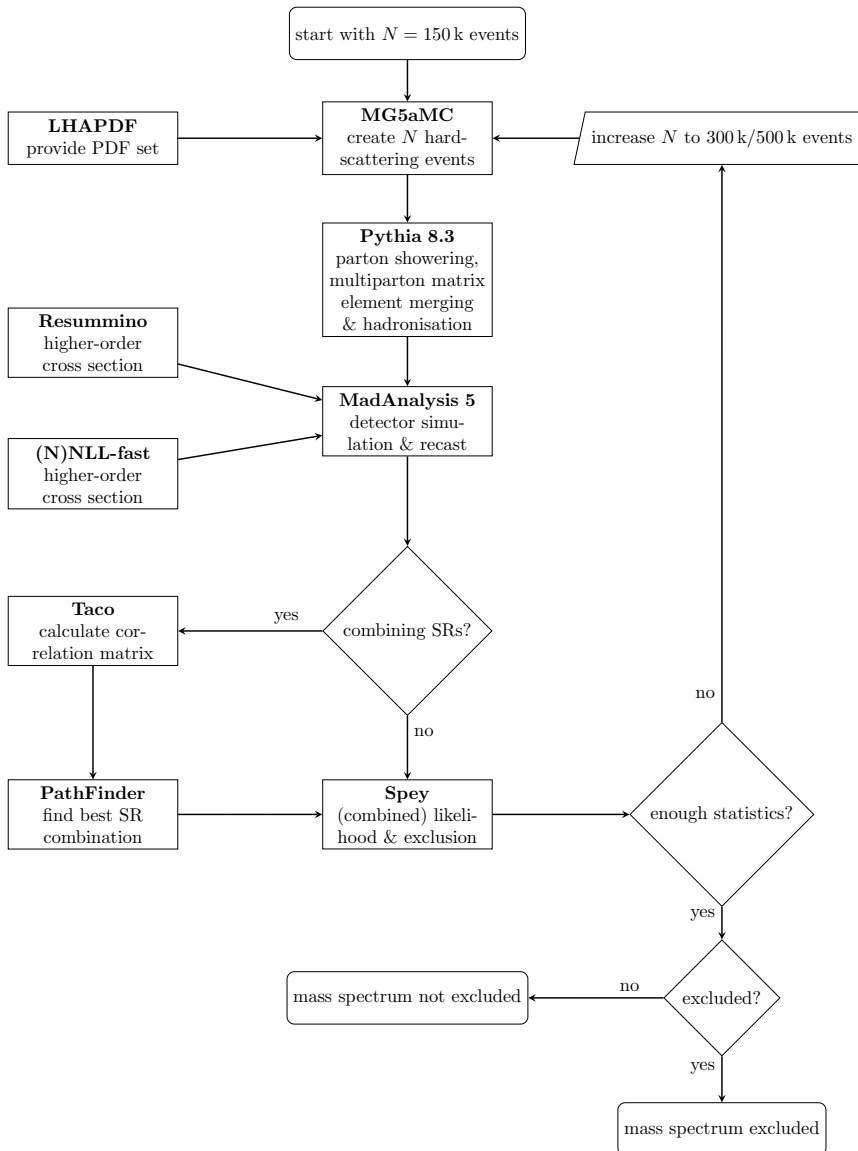


Figure 2: Flowchart diagram of the used toolchain.

next passed to the statistical tool **SPEY** [63], which uses a variety of likelihood-based prescriptions for hypothesis testing and the derivation of the confidence level of exclusion (CL) of a single SR, or of a combination of multiple SRs. Since the number of events surviving the cuts varies from SR to SR, if the number of events populating the SR with the highest exclusion power is too low ($\lesssim 50$ events), we regenerate events with increased statistics, first considering 300 k events, and next 500 k events if 300 k events are still insufficient.

Iterating this procedure scanning over the relevant mass points in the model parameter space, we obtain the 95% CL exclusion contour for the individual processes, as well as for their combination. The exclusion limits are calculated at first for the individual

Cuts	ATLAS	ATLAS	CMS	CMS
	EXOT-2018-06	CONF-2019-040	SUS-19-006	EXO-20-004
veto	e, μ, τ, γ	e, μ	e, μ, γ	$e, \mu, \tau, \gamma, b\text{-jet}$
N_j	≥ 1	≥ 2	≥ 2	≥ 1
E_T^{miss}	$> 200 \text{ GeV}$	$> 300 \text{ GeV}$	-	$> 250 \text{ GeV}$
$ \eta $	< 2.4	-	< 2.4	< 2.4
$p_T(j_1)$	$> 150 \text{ GeV}$	$> 200 \text{ GeV}$	-	$> 100 \text{ GeV}$
$p_T(j_2, \dots, j_{N_j})$	$> 30 \text{ GeV}$	$> 50 \text{ GeV}$	$> 30 \text{ GeV}$	$> 20 \text{ GeV}$
$\Delta\Phi(\text{jet}, \mathbf{p}_T^{\text{miss}})$	> 0.4	> 0.2	> 0.5	> 0.5
m_{eff}	-	$> 800 \text{ GeV}$	-	-
H_T	-	-	$> 300 \text{ GeV}$	-
$ \vec{H}_T^{\text{miss}} $	-	-	$> 300 \text{ GeV}$	-

Table 1: Summary of the event selection cuts of the four analyses ATLAS-EXOT-2018-06, ATLAS-CONF-2019-040, CMS-SUS-19-006 and CMS-EXO-20-004. Requirements include vetos on specific objects, as well as selections on the number of jets N_j , the amount of missing transverse energy E_T^{miss} , the pseudo-rapidity $|\eta|$ and transverse momentum p_T of the different jet candidates, the angular separation between the jets and the missing transverse momentum $\Delta\Phi(\text{jet}, \mathbf{p}_T^{\text{miss}})$, and the global observables defined in Eq. (3.2).

processes within each analysis, selecting the most sensitive SR as the one with the highest obtained exclusion value. This is further generalised to obtain the combined exclusion limits for the three sub-processes together. Further practical details (including information on the analyses considered and our limit setting procedure) are collected in Section 3.1 and Section 3.2.

3.1 Recast of single experimental analyses

All events generated, alongside their associated (resummed) cross sections, are passed to MA5 to reinterpret the results of four Run 2 ATLAS and CMS analyses at a centre-of-mass energy of $\sqrt{s} = 13 \text{ TeV}$. These analyses respectively account for integrated luminosities of 139 fb^{-1} and 137 fb^{-1} of data. Specifically, we investigate four searches that target jets and missing transverse momentum and that include SRs focusing not only on a monojet signature but also on a topology allowing for multiple hard jets. These searches are identified as ATLAS-EXOT-2018-06 [64], ATLAS-CONF-2019-040 [65], CMS-SUS-19-006 [66], and CMS-EXO-20-004 [67], and they have demonstrated the highest sensitivity to the considered simplified scenario. Details regarding their integration into MA5, along with corresponding validation notes, can be found on the MA5 dataverse [68–71], on the MA5 Public Analysis Database (PAD) [72], as well as in the works [67, 73–76]. The preselection criteria defining these four analyses are briefly summarised in Table 1.

These cuts have been devised to possibly observe the targeted BSM signal, which is

expected to be characterised by a significant production of events containing energetic jets, no leptons and a substantial amount of missing transverse energy E_T^{miss} . Although the acceptance cuts implemented in the four analyses are largely similar, they define different signal regions, thereby yielding varying sensitivities across the model parameter space. In particular, we firstly notice that the requirements on the minimal number of jets and their minimal transverse momentum $p_T(j)$ vary slightly. In this way, the CMS-EXO-20-004 analysis is sensitive to a softer monojet-like signature (thanks to lower cut thresholds) while the ATLAS-CONF-2019-040 search is blind in this region. Secondly, global cuts on the effective mass m_{eff} and the visible (H_T) and invisible (\vec{H}_T^{miss}) hadronic activity are only imposed in some of the considered analyses, that define these variables as

$$m_{\text{eff}} = E_T^{\text{miss}} + \sum_{p_T > 50 \text{ GeV}} p_T(j), \quad H_T = \sum_{|\eta| < 2.4} p_T(j), \quad \vec{H}_T^{\text{miss}} = \sum_{|\eta| < 5} \vec{p}_T(j). \quad (3.2)$$

The cuts on H_T and \vec{H}_T^{miss} implemented in the CMS-SUS-19-006 analysis imply a focus on a signal topology in which the hadronic activity originates from a large number of not necessarily very hard jets. In contrast, the ATLAS-EXOT-2018-06 search requires only one highly energetic jet, and optionally additional softer jets.

Using MA5, we calculate the number of signal events n_s expected to populate each SR of the four analyses. This information, together with the corresponding number of experimentally observed events n_{obs} , the number of expected SM background events n_b and the associated uncertainty Δn_b is passed to SPEY for statistical analysis. Using a general composite likelihood approach which employs Poisson distributed data, Gaussian-distributed nuisance and the so-called test statistic \tilde{q}_μ [77], SPEY computes separate CLs exclusion for each SR of each analysis and for the three sub-processes. To get exclusion limits for the combination of the three processes, we consider that each SR is populated by a number of events given by

$$n_s = n_s^{\tilde{q}\tilde{q}^*} + n_s^{\tilde{q}\tilde{\chi}_1^0} + n_s^{\tilde{\chi}_1^0\tilde{\chi}_1^0}, \quad (3.3)$$

where $n_s^{\tilde{q}\tilde{q}^*}$, $n_s^{\tilde{q}\tilde{\chi}_1^0}$ and $n_s^{\tilde{\chi}_1^0\tilde{\chi}_1^0}$ respectively denote the number of signal events expected for each of the three individual processes. We refer to Appendix B for more details.

3.2 Combining the analyses

The combination of the SRs of the four analyses requires to take into account their mutual correlations. For this purpose, we make use of MA5 to generate a binary $n_{\text{events}} \times n_{\text{SR}}$ matrix containing one row per event and one column per SR. A specific element of this matrix is either 1 or 0, depending on whether a given event populates the corresponding SR or not. This ‘acceptance’ matrix is next passed to TACO, which calculates the (Pearson) correlation coefficients between two SRs and generates a symmetric correlation matrix, *i.e.* an $n_{\text{SR}} \times n_{\text{SR}}$ matrix. Two SRs are flagged as uncorrelated if their correlation coefficient is smaller than 0.01, else their correlation is stored. Moreover, the correlation coefficients relating a signal region of an ATLAS analysis to a signal region of a CMS analysis are manually set to zero, because they rely on distinct data sets. This is however an optimistic

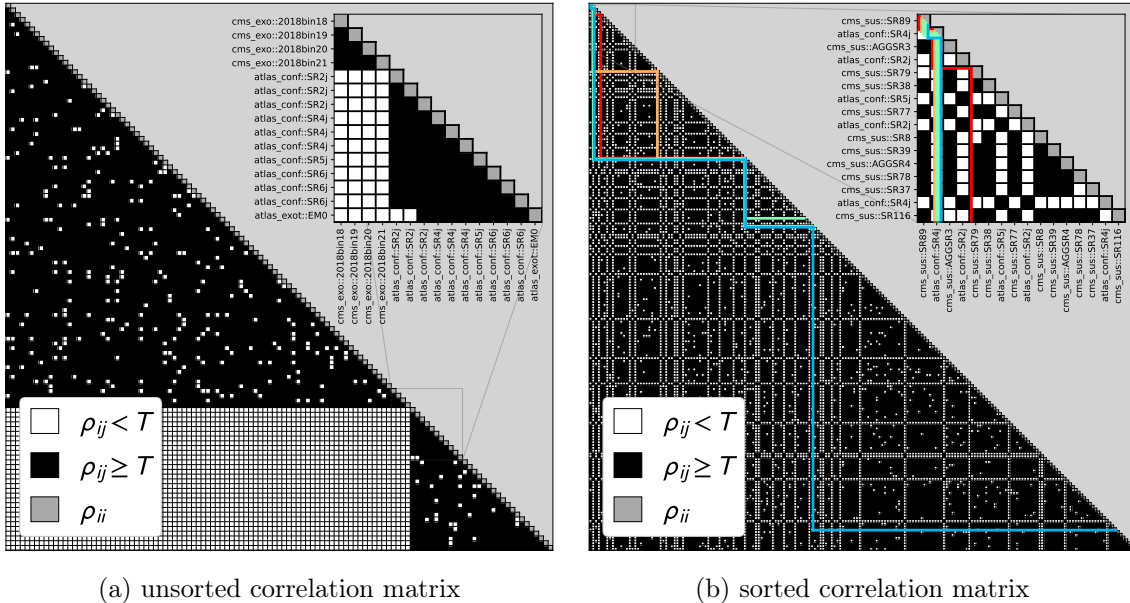


Figure 3: Correlation matrix ρ of a representative set of SRs of the four discussed analyses in case of squark pair production and a scenario with $m_{\tilde{\chi}_1^0} = 350$ GeV and $m_{\tilde{q}} = 1000$ GeV. Black and white dots respectively encode a correlated and an uncorrelated pair of SRs. We display the correlation matrix with SRs unsorted (left), as well as after sorting them in a way such that SRs with the highest weight come first (right). The combinations yielding the best sensitivity are highlighted through coloured paths.

approximation, as the two experiments may share some systematic uncertainties. In this case, any non-zero correlation would reduce the combined exclusion limit obtained [63].

The correlation matrix is then passed to the `PathFinder` software so that it could determine the most constraining combination of uncorrelated SRs. This is done by assigning to each SR a weight equal to the logarithm of the likelihood-ratios between the SUSY model tested and the background-only expectation, that is also proportional to the CLs exclusion. Since the likelihoods of multiple SRs combine multiplicatively, the log likelihood ratio associated with a subset of regions is simply given by the sum of their weights. The `PathFinder` package has been designed to identify the set of uncorrelated SRs with the highest accumulated weight.

In Fig. 3, we present various versions of the correlation matrix ρ obtained for squark pair production, considering an illustrative scenario with $m_{\tilde{\chi}_1^0} = 350$ GeV and $m_{\tilde{q}} = 1000$ GeV. First, we display the unsorted correlation matrix in Fig. 3a, where the SRs are arranged based on the order of their declarations in the analysis implementations. Notably, a block-shaped white area is observed in the lower-left part of the figure. Each of the elements of this block represents the intersection of an ATLAS SR and a CMS SR, which are enforced to be uncorrelated due to their association with different experiments. After sorting the columns and rows of the matrix ρ according to the calculated weight of its different elements, we obtain the structured matrix shown in Fig. 3b, with now lines of mostly only uncorrelated

regions instead of a block. The zoomed-in insets of the figures present results for a subset of SRs, identified by their names on the axes. It is evident that the majority of combinations within one analysis are correlated, but some uncorrelated options still exist.

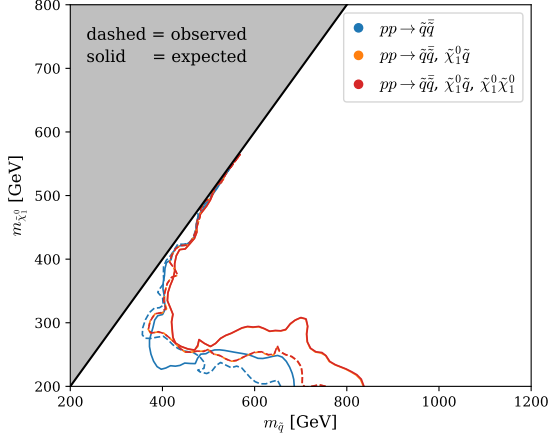
Utilising the path-finding algorithm, we identify the five best paths that combine the different regions in the most sensitive manner. A given path contains all SRs where the corresponding coloured line intersects the diagonal, with the red line denoting the most constraining combination. As can be seen from the zoomed-in inset, this best combination includes the two topmost and therefore most constraining individual SRs, and the fifth most constraining SR. This demonstrates that combinations of SRs of the same analysis can be realised (here CMS-SUS-19-006). These three SRs, as well as any set of SRs lying on a specific found path, are uncorrelated with each other (which is highlighted by the black-and-white color coding). This can be seen from explicitly looking at the correlations in the fifth row, showing that the fifth SR is uncorrelated with both the first and second SR. However, the most constraining combination does not necessarily have to include the most constraining SR, but can also start further down, depending on the calculated combined weights.

We hence demonstrate the existence of combinations of a few regions that have the potential to enhance sensitivity to the signal. This is discussed quantitatively in Section 4, after inputting the list of SRs corresponding to the most constraining path into the software tool `SPEY` to calculate exclusions. We note that to combine the three sub-processes considered, we need to construct the corresponding acceptance matrix with all generated events included. This is achieved through the merging of the three individual acceptance matrices along the ‘*event* axis’.

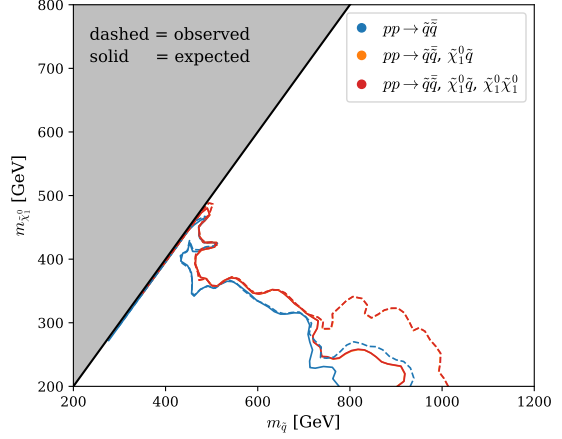
4 Results

In Fig. 4 (as well as in the tables provided in Appendix C), we focus on the bounds obtained from each of the four considered analyses individually. Expected (solid lines) and observed (dashed lines) 95% CL exclusion limits are presented in the $(m_{\tilde{q}}, m_{\tilde{\chi}_1^0})$ mass plane, and we compute them based on signal predictions determined as outlined in Section 3. The exclusion contours are computed by interpolating between the considered mass points (see Appendix C). Their smoothness and regularity is therefore a result of both the parameter space coverage regarding our simplified model of the considered analysis and the quality of the interpolation. Each figure showcases sensitivity contours distinguished by their colour coding. We compare bounds that are determined from a signal involving only strong production of a pair of squarks, each decaying into a neutralino and jets (blue). Such a signal definition matches how SUSY signals are simulated in experimental analyses up to now. Next, we examine the variation of the bounds when contributions from associated neutralino-squark production (orange) and neutralino-pair production (red) are included. We recall that these limits are derived by considering solely the most sensitive among all SRs within each analysis.

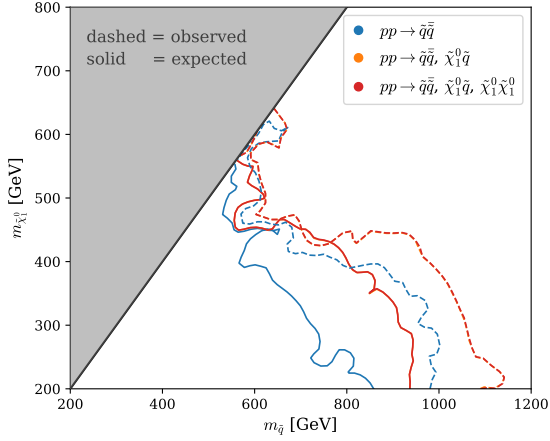
The ‘full’ bounds, incorporating all three sub-processes (red contours), largely coincide with the bounds derived from the combination of squark-pair and associated neutralino-



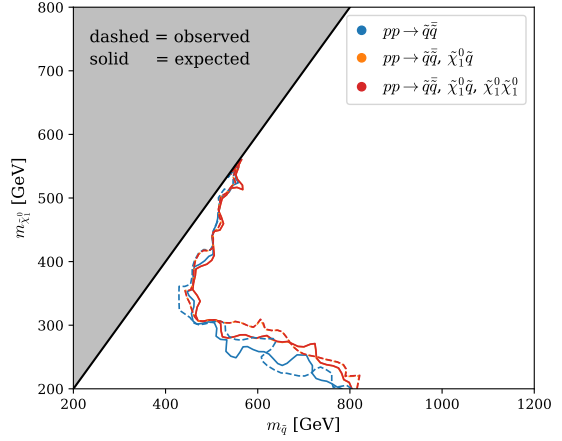
(a) ATLAS-EXOT-2018-06



(b) ATLAS-CONF-2019-040



(c) CMS-SUS-19-006



(d) CMS-EXO-20-004

Figure 4: Exclusion contours at 95% CL on the considered simplified model, presented in the squark and neutralino mass plane. Bounds have been obtained by the reinterpretation of the results of the ATLAS-EXOT-2018-06 (top left), ATLAS-CONF-2019-040 (top right), CMS-SUS-19-006 (bottom left) and CMS-EXO-20-004 (bottom right) analyses. We consider three scenarios for signal modelling: a signal involving only squark-pair production (blue), both squark-pair and associated neutralino-squark production (orange), and all three production sub-processes (red). Expected (solid) and observed (dashed) bounds are derived from the most constraining SR in each specific analysis.

squark production only (orange contours). This suggests that neutralino pair production has a marginal impact on the exclusions computed for a given mass spectrum. While the strong channel contributes dominantly, associated production has a non-negligible impact and therefore allows for a strengthening of the limits. This is particularly evident in the parameter space regions where the squark mass is large, and where, as already discussed in Section 2 regarding cross sections, squark-pair production begins to be phase-space sup-

pressed. For example, at $m_{\tilde{\chi}_1^0} = 250$ GeV, both observed and expected exclusion limits exhibit gains in squark mass of approximately 10 GeV for the CMS-EXO-20-004 analysis, and up to about 100 GeV for the other three analyses. These results reinforce the need for better and more accurate signal modelling in all existing LHC searches for SUSY, whenever it is computationally achievable.

Moreover, the four analyses demonstrate sensitivity to different regions in the parameter space, hinting at the potential to enhance overall sensitivity through their combination. Notably, the ATLAS-EXOT-2018-06 and CMS-SUS-19-006 analyses show increased sensitivity in the vicinity of the diagonal of the mass plane, where the squark-neutralino spectrum is compressed. In such scenarios, neutralinos emerging from squark decays carry almost all the squark energy so that the associated jets have low energy. Consequently, the overall jet multiplicity in the signal events is lower than in split mass configurations where highly-energetic jets could originate from squark decays. Furthermore, the CMS-SUS-19-006 analysis yields the strongest exclusion limits among all four analyses considered. Unlike the others, there is no requirement on the presence of a specific very highly energetic jet. Instead, it imposes constraints on global hadronic activity through the H_T variable defined in Eq. (3.2), ensuring that it surpasses a certain threshold. Consequently, this analysis allows for several jets with smaller transverse momentum to collectively fulfil the hadronic activity requirements, rather than relying on a single jet embedding the bulk of it. The dominant squark pair production channel typically leads to the production of at least two hard jets from squark decays, with the possibility of additional hadronic activity from QCD radiation, thereby meeting the analysis thresholds outlined in Table 1 without needing to rely on the presence of a very hard initial-state radiation. Thus, at this point, we conclude that analyses that are more inclusive in terms of jet energy and multiplicity are preferable to probe the considered MSSM-inspired simplified model.

The exclusion limits obtained by combining uncorrelated SRs from the four different analyses are depicted in Fig. 5 (as well as in the tables of Appendix C). Bounds are computed from the most sensitive combination of SRs determined by the `PathFinder` package, as detailed in Section 3.2. We analyse signal scenarios involving squark-pair production only (blue), and assess the impact of adding contributions from associated neutralino-squark production (orange) and neutralino-pair production (red). As above, neutralino-pair production has no discernible effect, as evidenced by the superposition of the red and orange contours. The comparison of the bounds computed from a signal comprising only squark-pair production, as currently modelled in experimental LHC analyses, to those derived from the full squark and neutralino signal, underscores once again the significant potential improvement achievable through better signal modelling including all contributing subprocesses, especially when the spectrum is not too compressed.

We compare these findings with limits derived from a signal including all three subprocesses, and utilising the most sensitive SR of the CMS-SUS-19-006 analysis (dashed contour). This comparison is motivated by the fact that the CMS-SUS-19-006 analysis has consistently emerged as the most constraining analysis (see Fig. 4). Combining multiple uncorrelated SRs of different analyses results in an additional gain in sensitivity compared to using the best SR from individual analyses to derive bounds, the gain being more pro-

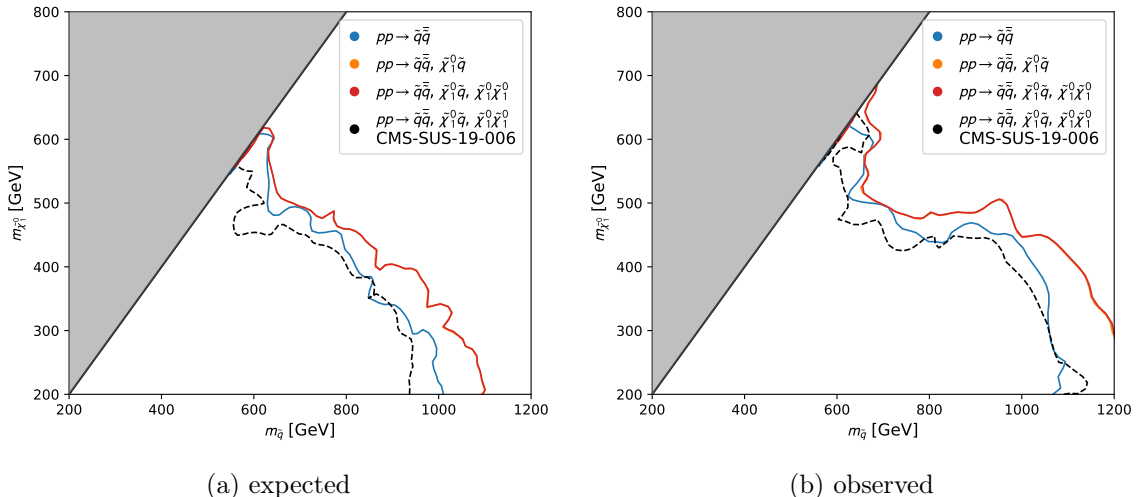
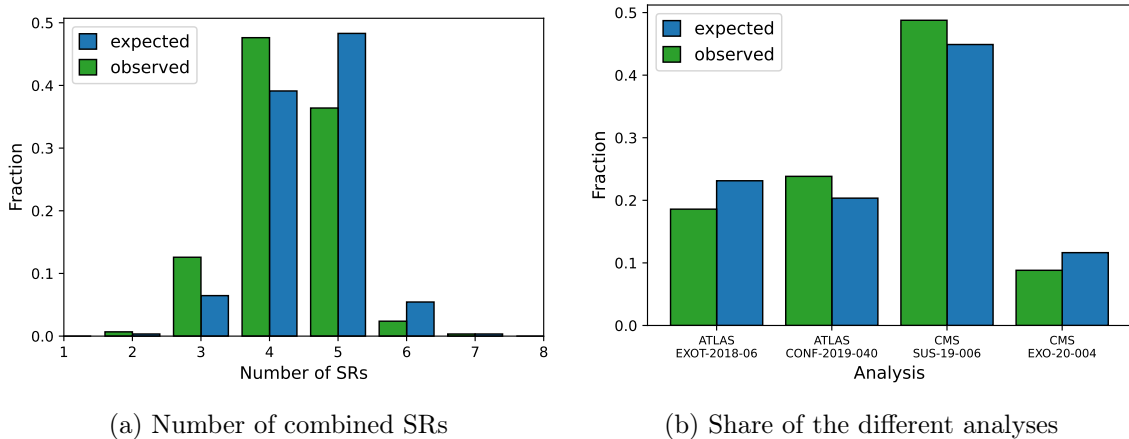


Figure 5: Expected (left) and observed (right) exclusion contours at 95% CL on the considered simplified model, presented in the squark and neutralino mass plane. Bounds have been derived from the most sensitive combination of uncorrelated SRs of the ATLAS-EXOT-2018-06, ATLAS-CONF-2019-040, CMS-SUS-19-006 and CMS-EXO-20-004 analyses. We consider three scenario for signal modelling: a signal involving only squark-pair production (blue), both squark-pair and associated neutralino-squark production (orange), and all three production sub-processes (red). For comparison, the exclusion contour determined from the most sensitive SR of the CMS-SUS-19-006 analysis is also shown (dashed, black).

nounced when the spectrum is more split. Bounds on squark masses typically increase by approximately 100 GeV for both expected and observed limits, reaching up to 200 GeV in certain regions of the parameter space. Notably, employing a conservative modelling of the SUSY signal including only squark-pair production together with the best combination of uncorrelated regions (blue contours) yields increased sensitivity compared to relying on the best signal modelling possible but without combining any SR. Thus, while improving signal modelling is important, correlating findings from different analyses or sub-analyses is equally, and possibly more, essential.

To understand the details of the SR combination process for the considered signal, we present in Fig. 6 the number of SRs combined according to the results of the **Pathfinder** algorithm (left panel). Additionally, we indicate, for each specific combination, the proportion of SRs originating from each individual analysis (right panel). In both cases, we normalise the results to the total number of scanned points in the parameter space. On average, four to five different SRs are combined in more than 90% of the cases, with the CMS-SUS-19-006 analysis contributing the most to this combination. This reflects the fact that this analysis is individually the most constraining, being more inclusive in its selection criteria (see also Table 1). However, it has a leading and determining impact only in half of the cases, highlighting the importance of exploiting information from other analyses as well. The average number of combined SRs that belong to the same analysis can be approximated by multiplying the average path length deduced from Fig. 6a with the rele-



(a) Number of combined SRs

(b) Share of the different analyses

Figure 6: Information on the combination of SRs across the parameter space. For each scanned mass point, we report the number of SRs combined (left), and the proportion of SRs originating from each individual analysis (right). The results are normalised to the total number of scanned points in the parameter space.

vant analysis fraction shown in Fig. 6b. This yields roughly 2.5 for the CMS-SUS-19-006 analysis, 1.0 for each of the considered ATLAS analyses, and 0.5 for the CMS-EXO-20-004 search.

While other analyses are generally less constraining than the CMS-SUS-19-006 analysis, they still substantially contribute to the combination. This is particularly true for the ATLAS-EXOT-2018-06 and ATLAS-CONF-2019-040 analyses, as ATLAS and CMS searches are naturally considered uncorrelated. Furthermore, although we might expect a reduced contribution from the monojet CMS-EXO-20-004 analysis due to its smaller relevance (as displayed in Fig. 4) and a likely stronger correlation with the CMS-SUS-19-006 analysis, its effects cannot be neglected. Therefore, we advocate for combining analyses whenever possible to ensure the best possible coverage of the parameter space with available data.

5 Conclusion

In this project, we focused on a simplified supersymmetric scenario inspired by the MSSM, where all superpartners are decoupled except for one squark flavour and a bino-like neutralino. Our objective was to demonstrate the gain in exclusion power achieved by combining uncorrelated SRs from different LHC searches for SUSY. Additionally, we aimed to illustrate the importance of improved signal modelling inherent to new physics setups in which several processes contribute. Our analysis encompasses four LHC searches targeting multiple jets and missing transverse energy, specifically the ATLAS-EXOT-2018-06, ATLAS-CONF-2019-040, CMS-SUS-19-006 and CMS-EXO-20-004 analyses. We considered a signal comprising squark-pair production, associated squark-neutralino production, as well as neutralino-pair production, that we modelled using state-of-the-art Monte Carlo

simulation techniques including multi-partonic matrix element merging and the most precise predictions to date for the corresponding cross sections.

We began by examining a signal incorporating squark-pair production only, consistent with what is achieved in Monte Carlo simulations relevant for current LHC searches. Our investigation revealed that the addition of associated squark-neutralino production significantly enhanced the exclusion power, corroborating recent findings. This effect is particularly pronounced when the SUSY spectrum is split and for neutralino masses below approximately 400 GeV. Furthermore, we observed that neutralino-pair production has minimal impact on the currently probed parameter space regions with the available data set. However, this may change in the future due to upcoming stronger squark and neutralino bounds, and the associated phase-space suppression of squark-pair and neutralino-squark production.

Combining uncorrelated SRs from different analyses further extends the reach of the searches considered. Notably, squark and neutralino mass bounds exceed those derived from individual analyses by approximately 100 GeV to 200 GeV. These results highlight the critical importance of combining SRs from different analyses, ideally within LHC collaborations when feasible, but also through innovative and approximate methods like the recently developed TACO approach utilised in this study and that could be employed outside the collaborations.

Acknowledgments

We thank Jack Araz for providing us with useful inputs regarding the SPEY package, as well as Humberto Reyes-Gonzalez and Jamie Yellen for their help with the Taco and the PathFinder software. We also thank Sabine Kraml for reading and commenting on the manuscript. BF acknowledges support from grant ANR-21-CE31-0013 (project DMwith-LLPatLHC) from the French *Agence Nationale de la Recherche* (ANR). Work in Münster is supported by the BMBF through project 05P21PMCAA and DFG through GRK 2149 and SFB 1225 “Isoquant,” project-id 273811115. JF acknowledges financial support from ICSC – Centro Nazionale di Ricerca in High Performance Computing, Big Data and Quantum Computing, funded by European Union – NextGenerationEU. Calculations (or parts of them) for this publication were performed on the HPC cluster PALMA II of the University of Münster, subsidised by the DFG (INST 211/667-1).

A Event generation and multi-partonic matrix element merging

In order to get an accurate description of the hadronic activity in events with a final state featuring a high jet multiplicity after parton showering, it is essential to rely on the combination of hard-scattering matrix elements possibly featuring additional QCD radiation. Consistency in this combination is crucial to avoid double counting the QCD emissions generated from the matrix elements (describing exclusive final states with a fixed number of jets) and from parton showers (describing inclusive final states in the number of jets). We achieve this by following the CKKW-L merging prescription [55–57]. In practice, the

algorithm starts from a hard-scattering event and generates a sequence of dipole emissions resembling the structure emerging from the showered event. If the configuration of any of the dipole emissions falls into the phase space region that should be described by the matrix element, the event is rejected. This ensures that the hardest emissions are always described by matrix elements and the softer ones by parton showers. Analogously, this results in re-weighting the event by the associated Sudakov form factor (*i.e.* the probability that there is no further emission once we start from the matrix element configuration). Each dipole emission in the sequence is thus accepted as long as its scale does not exceed a predefined merging scale Q_{MS} , that describes the transition between the regime in which QCD radiation is described by matrix elements and that in which it is described by parton showers.

Differential jet rate (DJR) distributions play an important role in validating the choice of parameters relevant for the merging prescription, particularly the value of Q_{MS} to which they are highly sensitive. A suitable choice ensures a smooth transition between an event topology with $n - 1$ final-state hard jets and a topology with n final-state hard jets, without any bumps, peaks or abrupt transitions in the DJR spectra. However, default settings in **MG5aMC** often result in bumps indicative of resonances for the considered signal. These bumps stem from certain diagrams exhibiting the exchange of intermediate s -channel off-shell squarks that see their off-shell nature modified by QCD radiation. To address this issue, the `bwcutoff` parameter in the **MG5aMC** configuration card has to be increased from 15 to, for example, 35. This adjustment implies that squarks are flagged as on-shell in a wider region around their pole mass, which further impacts cutting out their contributions in processes featuring neutralinos in the final state (see Section 2).

We validated the merging prescription for a variety of different mass combinations, that we illustrate for the case $m_{\tilde{\chi}_1^0} = 200 \text{ GeV}$ and $m_{\tilde{q}} = 600 \text{ GeV}$ in Fig. 7. We present, for neutralino-pair (top row), squark-neutralino (middle row) and squark-pair (bottom row) production, total DJR spectra (green), together with the individual contributions emerging from matrix elements featuring no extra jet (blue), one extra jet (orange) and two extra jets (purple). For completeness, we provide below the associated **MG5aMC** commands that we use to test associated neutralino-squark production (the commands for the other channels being similar):

```
define squa = ur ur~
generate p p > n1 ur $squa, ur > u n1 @1
add process p p > n1 ur~ $squa, ur~ > u~ n1 @1
add process p p > n1 ur j $squa, ur > u n1 @2
add process p p > n1 ur~ j $squa, ur~ > u~ n1 @2
add process p p > n1 ur j j $squa, ur > u n1 @3
add process p p > n1 ur~ j j $squa, ur~ > u~ n1 @3
output
launch

shower = Pythia8
```

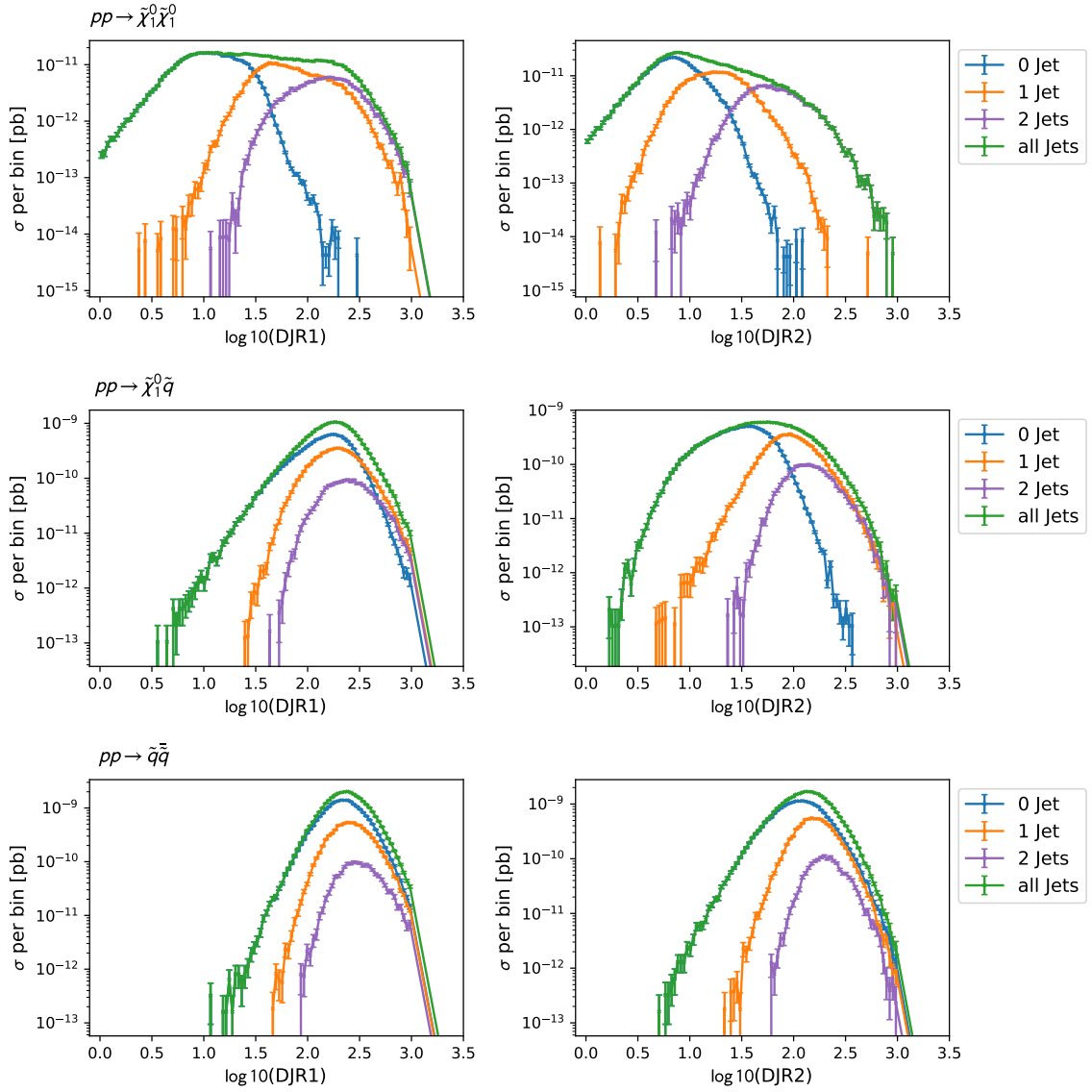


Figure 7: DJR distributions for the three different processes considered, and a scenario defined by $m_{\tilde{\chi}_1^0} = 200$ GeV and $m_{\tilde{q}} = 600$ GeV.

```

set pldlabel = lhpdf
set lhaid = 27000
set ebeam1 = 6500.0
set ebeam2 = 6500.0
set use_syst = False
set nevents = 500000
set mass mneu1 200.0
set mass msu4 600.0
set mass msd1 30000

```

```

set mass msd2 30000
...                               #all other SUSY masses decoupled
set mass msn2 30000
set mass msn3 30000
set wsu4 auto
set rnn1x1 1
set rnn2x2 1
set rnn1x2 0
set rnn1x3 0
...                               #all other entries set to 0
set rnn4x3 0
set rnn4x4 0
set Merging:nJetMax 2
set ktdurham = -1
set Merging:mayRemoveDecayProducts = on
set Merging:doPTLundMerging=on
set Merging:Process=pp>n1,ur,ur~
set ptlund = 100.0                #ptlund=1/8 (m_squark+m_neutralino)
set bwcutoff = 35.0

```

We can note that we have explicitly chosen the merging scale to one quarter of the SUSY hard scale as given in Eq. (3.1).

B Statistical analysis

Within the SPEY framework [63], the likelihood function for signal exclusion is expressed as

$$\mathcal{L}(\mu, \theta) = \text{Pois}(n_{\text{obs}} | \mu n_s + n_b + \theta \cdot \Delta n_b) \text{Gauss}(\theta | 0, 1). \quad (\text{B.1})$$

Here, μ represents the signal strength, indicating in our case the presence ($\mu = 1$) or absence ($\mu = 0$) of a SUSY signal. The parameter θ serves as a single nuisance parameter and captures how results can deviate from the SM expectation in terms of standard deviations. In this formulation, the likelihood function comprises two components. The Poisson-distributed factor accounts for the observed number of events given the expected contributions from both signal n_s and background n_b , along with the impact of the nuisance parameter that multiplies the uncertainty in the background estimation denoted by Δn_b . Furthermore, a unit Gaussian distribution is used for the constraint factor to model uncertainties in the background estimation.

The SUSY signal hypothesis is tested using the test statistic \tilde{q}_μ [77], defined by

$$\tilde{q}_\mu = \begin{cases} -2 \log \frac{\mathcal{L}(\mu, \theta_\mu)}{\mathcal{L}(0, \theta_0)} & \text{if } \hat{\mu} < 0, \\ -2 \log \frac{\mathcal{L}(\mu, \theta_\mu)}{\mathcal{L}(\hat{\mu}, \hat{\theta})} & \text{if } 0 \leq \hat{\mu} \leq \mu, \\ 0 & \text{if } \mu < \hat{\mu}, \end{cases} \quad (\text{B.2})$$

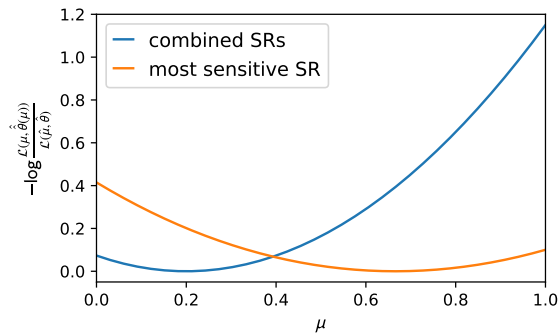


Figure 8: Negative logarithmic likelihood ratio as a function of the signal strength μ when using the most sensitive SR from all analyses (orange) and the most sensitive combination of SRs as returned by the `PathFinder` algorithm. We consider squark-pair production for $m_{\tilde{\chi}_1^0} = 250$ GeV and $m_{\tilde{q}} = 1000$ GeV.

where $\hat{\mu}$ and $\hat{\theta}$ denote the set of parameters that maximises the likelihood (representing thus the best fit to the data), and θ_μ is the nuisance parameter value that maximises the likelihood for a given signal strength μ . The corresponding p -value (allowing to deduce an exclusion confidence level CL) is therefore given by

$$p_{\tilde{q}_\mu} = \int_{-\infty}^{\sqrt{\tilde{q}_\mu} - \sqrt{\tilde{q}_{\mu,A}}} f(\tilde{q}'_\mu, \mu) d\tilde{q}'_\mu, \quad (\text{B.3})$$

where the test statistics $\tilde{q}_{\mu,A}$ is obtained assuming Asimov data and $f(\tilde{q}'_\mu, \mu)$ corresponds to the \tilde{q}_μ probability distribution. Consequently, an increasing incompatibility between an hypothesised signal strength μ and the observed one $\hat{\mu}$ would lead to a decreasing likelihood ratio, resulting in an increasing test statistic and a higher corresponding CL.

We compute both the background-only exclusion confidence level CL_b (with $\mu = 0$) and the signal-plus-background exclusion confidence level CL_{s+b} (with $\mu = 1$). The ratio $\text{CL}_s = \text{CL}_{s+b}/\text{CL}_b$ then yields the observed p -value. We obtain the expected p -value (referred to as the ‘*a posteriori*’ p -value in `SPEY`) by replacing the observed number of events with the expected number of SM events based on background predictions and uncertainties.

The effect of combining uncorrelated SRs is evaluated by multiplying their likelihoods,

$$\mathcal{L}_{\text{combined}}(\mu) = \prod_{i \in \text{SRs}} \mathcal{L}_i(\mu, \theta_i). \quad (\text{B.4})$$

This enables the calculation of logarithmic likelihood ratios (LLRs) by simple addition, which justifies the weighting assigned by the `PathFinder` algorithm as discussed in Section 3.2. The impact of combining SRs on the likelihood is illustrated in Fig. 8 for a scenario with $m_{\tilde{\chi}_1^0} = 250$ GeV and $m_{\tilde{q}} = 1000$ GeV, considering a signal comprising only squark-pair production. We compare the LLR associated with the most sensitive SR from all analyses considered (orange) to that obtained with the most sensitive combination of SRs determined by the `PathFinder` algorithm (blue). For $\mu = 1$ (the BSM signal hypothesis),

the combined LLR exceeds that of the single most sensitive SR, indicating a greater discrepancy between data and the signal-plus-background hypothesis and leading to a higher exclusion CL. Similarly, the shift of the minimum of the LLR as a function of μ towards lower μ values suggests that the data is more consistent with the SM hypothesis ($\mu = 0$).

C Tables

$m_{\tilde{\chi}_1^0}/m_{\tilde{q}}$ GeV	$\tilde{q}\tilde{q}$					$\tilde{q}\tilde{q} - \tilde{\chi}\tilde{q}$					$\tilde{q}\tilde{q} - \tilde{\chi}\tilde{q} - \tilde{\chi}\tilde{\chi}$				
	AC	AE	CS	CE	<i>cmb.</i>	AC	AE	CS	CE	<i>cmb.</i>	AC	AE	CS	CE	<i>cmb.</i>
200/900	0.88	0.68	0.92	0.61	0.99	0.95	0.86	0.99	0.79	1.0	0.95	0.86	0.99	0.79	1.0
200/1000	0.78	0.54	0.78	0.47	0.97	0.89	0.72	0.86	0.59	0.99	0.89	0.73	0.86	0.59	0.99
200/1200	0.53	0.27	0.59	0.24	0.73	0.67	0.45	0.71	0.39	0.91	0.68	0.45	0.72	0.4	0.91
200/1300	0.46	0.26	0.5	0.25	0.66	0.59	0.42	0.66	0.43	0.84	0.59	0.42	0.66	0.43	0.85
250/750	0.9	0.85	0.99	0.8	1.0	0.94	0.95	1.0	0.91	1.0	0.94	0.95	1.0	0.91	1.0
250/850	0.9	0.74	0.98	0.79	1.0	0.95	0.9	0.99	0.9	1.0	0.95	0.9	0.99	0.9	1.0
250/940	0.82	0.56	0.96	0.57	0.99	0.91	0.77	0.96	0.73	1.0	0.91	0.78	0.96	0.73	1.0
250/950	0.79	0.58	0.75	0.49	0.95	0.88	0.75	0.88	0.66	0.98	0.88	0.75	0.88	0.67	0.98
250/1000	0.76	0.51	0.75	0.38	0.93	0.86	0.69	0.83	0.55	0.99	0.86	0.7	0.83	0.55	0.99
250/1050	0.68	0.48	0.82	0.5	0.92	0.79	0.67	0.83	0.61	0.96	0.79	0.67	0.83	0.61	0.96
250/1080	0.62	0.42	0.65	0.33	0.87	0.78	0.6	0.82	0.46	0.95	0.78	0.6	0.82	0.46	0.96
250/1100	0.72	0.39	0.62	0.3	0.87	0.75	0.55	0.74	0.45	0.92	0.75	0.55	0.75	0.45	0.92
300/750	0.84	0.79	0.99	0.73	1.0	0.93	0.9	1.0	0.86	1.0	0.93	0.9	1.0	0.87	1.0
300/850	0.84	0.68	0.94	0.7	1.0	0.87	0.83	0.98	0.81	1.0	0.87	0.83	0.98	0.82	1.0
300/900	0.83	0.61	0.96	0.72	0.99	0.91	0.78	0.99	0.8	1.0	0.91	0.78	0.99	0.8	1.0
300/1000	0.68	0.48	0.77	0.41	0.9	0.78	0.66	0.84	0.56	0.95	0.78	0.66	0.84	0.57	0.96
300/1200	0.46	0.27	0.53	0.25	0.66	0.58	0.44	0.65	0.37	0.79	0.58	0.44	0.65	0.37	0.79
350/650	0.87	0.68	1.0	0.67	1.0	0.95	0.81	1.0	0.77	1.0	0.95	0.81	1.0	0.77	1.0
350/700	0.75	0.7	0.99	0.7	1.0	0.86	0.84	1.0	0.82	1.0	0.86	0.84	1.0	0.83	1.0
350/800	0.77	0.59	0.93	0.64	0.99	0.84	0.75	1.0	0.78	1.0	0.84	0.75	1.0	0.78	1.0
350/850	0.66	0.58	0.89	0.56	0.95	0.78	0.73	0.95	0.67	0.99	0.78	0.73	0.95	0.68	0.99
350/900	0.69	0.49	0.82	0.48	0.93	0.81	0.69	0.92	0.63	0.99	0.81	0.69	0.92	0.63	0.99
350/1000	0.64	0.4	0.64	0.45	0.89	0.74	0.56	0.73	0.53	0.94	0.74	0.57	0.73	0.53	0.94
350/1100	0.5	0.31	0.6	0.45	0.82	0.59	0.42	0.65	0.51	0.84	0.6	0.43	0.65	0.51	0.84
400/600	0.75	0.45	1.0	0.64	1.0	0.87	0.57	1.0	0.83	1.0	0.87	0.57	1.0	0.83	1.0
400/750	0.83	0.5	0.97	0.68	0.99	0.87	0.67	0.99	0.74	1.0	0.87	0.68	0.99	0.74	1.0
400/800	0.61	0.49	0.9	0.6	0.97	0.71	0.66	0.95	0.69	0.99	0.71	0.66	0.95	0.69	0.99
400/850	0.59	0.49	0.85	0.45	0.92	0.68	0.63	0.9	0.57	0.96	0.68	0.63	0.9	0.58	0.96
400/870	0.52	0.48	0.77	0.42	0.92	0.65	0.64	0.87	0.59	0.94	0.65	0.64	0.87	0.59	0.94
400/920	0.59	0.41	0.8	0.41	0.93	0.72	0.57	0.89	0.58	0.95	0.72	0.57	0.89	0.59	0.95
400/950	0.59	0.4	0.81	0.5	0.89	0.71	0.56	0.82	0.59	0.95	0.71	0.56	0.82	0.59	0.95
400/1000	0.54	0.33	0.65	0.46	0.77	0.62	0.48	0.72	0.5	0.9	0.62	0.48	0.72	0.5	0.9
400/1200	0.38	0.27	0.42	0.26	0.57	0.52	0.38	0.56	0.35	0.76	0.52	0.38	0.56	0.35	0.77
450/550	0.17	0.29	1.0	0.52	1.0	0.17	0.51	1.0	0.87	1.0	0.17	0.51	1.0	0.87	1.0
450/600	0.17	0.27	1.0	0.49	1.0	0.17	0.39	1.0	0.55	1.0	0.17	0.4	1.0	0.55	1.0
450/650	0.6	0.25	1.0	0.42	1.0	0.71	0.36	1.0	0.49	1.0	0.71	0.36	1.0	0.5	1.0
450/820	0.17	0.38	0.8	0.42	0.89	0.17	0.51	0.89	0.5	0.96	0.17	0.52	0.89	0.5	0.96
450/850	0.17	0.37	0.84	0.42	0.9	0.17	0.5	0.85	0.49	0.93	0.17	0.5	0.85	0.49	0.93
450/950	0.17	0.33	0.72	0.31	0.87	0.17	0.45	0.72	0.42	0.95	0.17	0.46	0.72	0.42	0.95
500/520	0.79	0.69	1.0	0.94	1.0	0.84	0.77	1.0	0.95	1.0	0.84	0.77	1.0	0.95	1.0
500/600	0.17	0.3	0.99	0.5	1.0	0.17	0.38	0.99	0.89	1.0	0.17	0.39	0.99	0.89	1.0
500/650	0.17	0.17	0.79	0.61	0.92	0.17	0.26	0.89	0.64	0.98	0.17	0.26	0.9	0.64	0.98
500/700	0.17	0.22	0.84	0.22	0.93	0.17	0.3	0.85	0.32	0.94	0.17	0.3	0.85	0.32	0.94
500/750	0.17	0.23	0.86	0.35	0.6	0.17	0.3	0.87	0.41	0.67	0.17	0.3	0.87	0.41	0.67
500/800	0.17	0.24	0.74	0.26	0.82	0.17	0.35	0.84	0.42	0.93	0.17	0.35	0.84	0.42	0.93
500/850	0.48	0.28	0.68	0.29	0.79	0.52	0.38	0.75	0.36	0.9	0.52	0.38	0.75	0.36	0.9
500/950	0.39	0.25	0.57	0.25	0.72	0.44	0.35	0.66	0.33	0.79	0.44	0.36	0.66	0.33	0.79
550/700	0.41	0.14	0.64	0.33	0.72	0.46	0.23	0.71	0.37	0.87	0.46	0.23	0.71	0.37	0.87
550/750	0.41	0.11	0.54	0.3	0.69	0.47	0.18	0.61	0.33	0.75	0.48	0.18	0.61	0.33	0.75
550/800	0.5	0.17	0.72	0.19	0.81	0.53	0.24	0.78	0.29	0.89	0.53	0.24	0.78	0.29	0.89
550/850	0.43	0.17	0.92	0.22	0.94	0.47	0.25	0.92	0.26	0.95	0.47	0.25	0.92	0.26	0.95
550/900	0.31	0.2	0.56	0.18	0.65	0.34	0.28	0.59	0.24	0.76	0.34	0.28	0.59	0.24	0.76
600/650	0.56	0.2	0.89	0.32	0.94	0.6	0.28	0.89	0.36	0.93	0.6	0.28	0.89	0.36	0.93
600/750	0.37	0.09	0.48	0.15	0.6	0.4	0.16	0.56	0.22	0.72	0.4	0.16	0.56	0.22	0.72
600/850	0.29	0.11	0.5	0.24	0.56	0.35	0.17	0.55	0.27	0.7	0.35	0.17	0.55	0.27	0.7
600/1000	0.31	0.17	0.31	0.19	0.48	0.35	0.22	0.38	0.23	0.53	0.35	0.22	0.38	0.23	0.53
600/1200	0.2	0.12	0.32	0.13	0.41	0.25	0.18	0.32	0.18	0.45	0.25	0.18	0.32	0.18	0.45
625/750	0.35	0.06	0.55	0.14	0.62	0.39	0.14	0.6	0.18	0.7	0.39	0.14	0.6	0.18	0.7
650/800	0.29	0.07	0.36	0.16	0.46	0.34	0.12	0.42	0.19	0.61	0.34	0.12	0.42	0.19	0.61
650/850	0.28	0.06	0.5	0.38	0.56	0.31	0.11	0.51	0.4	0.66	0.31	0.11	0.51	0.4	0.66
700/705	0.24	0.51	0.61	0.5	0.74	0.32	0.56	0.7	0.53	0.85	0.32	0.56	0.7	0.53	0.85
700/720	0.31	0.27	0.57	0.62	0.67	0.47	0.41	0.57	0.68	0.77	0.47	0.41	0.57	0.68	0.77
800/805	0.1	0.19	0.22	0.24	0.32	0.14	0.3	0.33	0.48	0.57	0.14	0.3	0.33	0.48	0.57
800/850	0.08	0.11	0.34	0.18	0.37	0.13	0.13	0.35	0.2	0.47	0.13	0.13	0.35	0.2	0.47
800/1200	0.09	0.04	0.1	0.05	0.14	0.12	0.06	0.13	0.07	0.19	0.12	0.06	0.13	0.07	0.19

Table 2: Subset of expected CLs for squark-pair production ($\tilde{q}\tilde{q}$) only, and after combining with neutralino-squark production ($\tilde{q}\tilde{q} - \tilde{\chi}\tilde{q}$) and neutralino pair-production ($\tilde{q}\tilde{q} - \tilde{\chi}\tilde{q} - \tilde{\chi}\tilde{\chi}$). We consider the ATLAS-CONF-2019-040 (AC), ATLAS-EXOT-2018-06 (AE), CMS-SUS-19-006 (CS) and CMS-EXO-20-004 (CE) analyses, as well as their combination (*cmb.*).

$m_{\chi_1^0}/m_{\tilde{q}}$	$\tilde{c}\tilde{q}$					$\tilde{q}\tilde{q} - \tilde{\chi}\tilde{q}$					$\tilde{q}\tilde{q} - \tilde{\chi}\tilde{q} - \tilde{\chi}\tilde{\chi}$				
	AC	AE	CS	CE	<i>cmb.</i>	AC	AE	CS	CE	<i>cmb.</i>	AC	AE	CS	CE	<i>cmb.</i>
200/900	0.96	0.63	1.0	0.61	1.0	0.99	0.83	1.0	0.76	1.0	0.99	0.83	1.0	0.76	1.0
200/950	0.94	0.64	0.97	0.57	1.0	0.98	0.8	1.0	0.69	1.0	0.98	0.8	0.99	0.69	1.0
200/970	0.92	0.64	0.96	0.65	0.99	0.98	0.8	0.99	0.91	1.0	0.98	0.81	0.99	0.91	1.0
200/1000	0.91	0.68	0.94	0.69	0.99	0.96	0.83	0.98	0.76	1.0	0.96	0.84	0.99	0.76	1.0
200/1050	0.85	0.63	0.89	0.7	0.97	0.92	0.8	0.97	0.81	1.0	0.92	0.81	0.97	0.81	1.0
200/1200	0.74	0.42	0.7	0.48	0.88	0.81	0.59	0.88	0.69	0.97	0.81	0.6	0.88	0.69	0.97
200/1300	0.69	0.43	1.0	0.38	0.82	0.8	0.6	1.0	0.7	0.95	0.8	0.61	1.0	0.7	0.95
250/750	0.94	0.54	1.0	0.84	1.0	0.98	0.81	1.0	0.94	1.0	0.98	0.81	1.0	0.94	1.0
250/850	0.97	0.54	0.99	0.74	1.0	0.99	0.72	1.0	0.86	1.0	0.99	0.72	1.0	0.86	1.0
250/940	0.93	0.55	0.99	0.59	1.0	0.97	0.76	0.99	0.77	1.0	0.97	0.76	0.99	0.77	1.0
250/950	0.91	0.59	0.96	0.65	0.99	0.96	0.75	0.99	0.73	1.0	0.96	0.75	0.99	0.73	1.0
250/1000	0.9	0.57	0.94	0.67	0.99	0.95	0.77	1.0	0.79	1.0	0.95	0.77	1.0	0.8	1.0
250/1050	0.85	0.63	0.89	0.7	0.99	0.91	0.79	0.96	0.8	1.0	0.91	0.79	0.96	0.8	1.0
250/1080	0.79	0.58	0.85	0.61	0.96	0.87	0.74	0.95	0.74	0.99	0.87	0.74	0.95	0.74	0.99
250/1100	0.76	0.54	0.83	0.62	0.95	0.85	0.7	0.94	0.72	0.98	0.85	0.7	0.94	0.72	0.98
300/750	0.88	0.48	1.0	0.83	1.0	0.94	0.71	1.0	0.9	1.0	0.94	0.72	1.0	0.9	1.0
300/850	0.91	0.44	0.99	0.7	1.0	0.95	0.64	1.0	0.82	1.0	0.96	0.64	1.0	0.82	1.0
300/900	0.93	0.51	0.98	0.57	1.0	0.97	0.67	1.0	0.71	1.0	0.97	0.67	1.0	0.72	1.0
300/1000	0.85	0.52	0.92	0.66	0.98	0.91	0.69	0.97	0.74	0.99	0.91	0.69	0.98	0.74	1.0
300/1200	0.64	0.38	0.69	0.5	0.72	0.72	0.54	0.86	0.61	0.95	0.72	0.54	0.86	0.61	0.95
350/650	0.88	0.32	1.0	0.86	1.0	0.95	0.55	1.0	0.92	1.0	0.95	0.55	1.0	0.92	1.0
350/700	0.76	0.45	0.99	0.83	1.0	0.87	0.62	1.0	0.89	1.0	0.87	0.62	1.0	0.89	1.0
350/800	0.82	0.38	0.98	0.75	1.0	0.93	0.59	1.0	0.85	1.0	0.93	0.59	1.0	0.85	1.0
350/850	0.84	0.33	0.98	0.64	1.0	0.91	0.53	0.99	0.74	1.0	0.91	0.53	0.99	0.74	1.0
350/900	0.86	0.42	0.96	0.55	0.98	0.92	0.57	0.99	0.68	1.0	0.92	0.58	0.99	0.68	1.0
350/1000	0.83	0.45	0.91	0.55	0.98	0.88	0.59	0.96	0.64	0.99	0.88	0.6	0.96	0.64	0.99
350/1100	0.72	0.45	0.81	0.59	0.92	0.79	0.57	0.9	0.64	0.97	0.8	0.58	0.9	0.64	0.97
400/600	0.73	0.32	1.0	0.88	1.0	0.92	0.52	1.0	0.91	1.0	0.92	0.52	1.0	0.91	1.0
400/750	0.84	0.24	0.97	0.62	0.99	0.88	0.4	0.99	0.72	1.0	0.88	0.4	0.99	0.72	1.0
400/800	0.64	0.31	0.94	0.67	0.99	0.77	0.48	0.98	0.74	0.99	0.77	0.49	0.98	0.74	0.99
400/850	0.76	0.3	0.95	0.52	0.98	0.85	0.48	0.98	0.63	1.0	0.85	0.49	0.98	0.63	1.0
400/870	0.74	0.28	0.95	0.58	0.98	0.83	0.44	0.98	0.72	1.0	0.83	0.45	0.98	0.72	1.0
400/920	0.78	0.3	0.94	0.53	0.98	0.85	0.44	0.97	0.62	0.99	0.85	0.44	0.97	0.63	0.99
400/950	0.79	0.35	0.92	0.45	0.98	0.87	0.54	0.97	0.58	0.99	0.87	0.54	0.97	0.59	0.99
400/1000	0.76	0.33	0.87	0.86	0.97	0.81	0.48	0.94	0.89	0.99	0.81	0.49	0.94	0.89	0.99
400/1200	0.56	0.36	0.69	0.41	0.81	0.67	0.49	0.83	0.52	0.93	0.67	0.49	0.83	0.52	0.93
450/550	0.38	0.38	1.0	0.54	1.0	0.38	0.6	1.0	0.78	1.0	0.38	0.6	1.0	0.78	1.0
450/600	0.38	0.23	1.0	0.56	1.0	0.38	0.35	1.0	0.61	1.0	0.38	0.36	1.0	0.61	1.0
450/650	0.59	0.22	1.0	0.48	1.0	0.7	0.37	1.0	0.56	1.0	0.7	0.37	1.0	0.57	1.0
450/820	0.38	0.18	0.86	0.48	0.93	0.38	0.38	0.93	0.56	0.99	0.38	0.38	0.93	0.56	1.0
450/850	0.38	0.36	0.9	0.52	0.96	0.38	0.47	0.95	0.57	0.98	0.38	0.47	0.95	0.57	0.98
450/950	0.38	0.26	0.9	0.46	0.95	0.38	0.39	0.94	0.57	0.99	0.38	0.39	0.94	0.57	0.99
500/520	0.83	0.44	1.0	0.92	1.0	0.87	0.59	1.0	0.94	1.0	0.87	0.59	1.0	0.94	1.0
500/600	0.38	0.18	1.0	0.49	1.0	0.38	0.33	1.0	0.64	1.0	0.38	0.34	1.0	0.64	1.0
500/650	0.38	0.31	0.82	0.43	0.96	0.38	0.43	0.91	0.5	0.97	0.38	0.43	0.91	0.5	0.97
500/700	0.38	0.14	0.88	0.41	0.94	0.38	0.34	0.89	0.47	0.95	0.38	0.35	0.89	0.47	0.95
500/750	0.38	0.18	0.8	0.51	0.88	0.38	0.33	0.87	0.56	0.9	0.38	0.33	0.87	0.56	0.9
500/800	0.38	0.19	0.74	0.58	0.74	0.38	0.34	0.85	0.63	0.93	0.38	0.34	0.85	0.63	0.94
500/850	0.5	0.15	0.8	0.48	0.93	0.58	0.3	0.88	0.54	0.92	0.58	0.3	0.88	0.54	0.92
500/950	0.58	0.22	0.84	0.4	0.93	0.66	0.32	0.9	0.48	0.96	0.66	0.32	0.9	0.48	0.96
550/700	0.4	0.17	0.69	0.34	0.77	0.44	0.27	0.81	0.41	0.87	0.44	0.28	0.81	0.41	0.87
550/750	0.39	0.17	0.69	0.43	0.79	0.47	0.3	0.79	0.46	0.89	0.47	0.3	0.79	0.46	0.89
550/800	0.54	0.12	0.79	0.36	0.87	0.62	0.38	0.82	0.42	0.93	0.62	0.39	0.82	0.42	0.93
550/850	0.47	0.13	0.85	0.39	0.88	0.52	0.24	0.85	0.45	0.85	0.52	0.24	0.85	0.45	0.85
550/900	0.4	0.12	0.73	0.32	0.83	0.49	0.21	0.82	0.39	0.84	0.49	0.21	0.82	0.39	0.84
600/650	0.54	0.34	0.97	0.37	0.98	0.58	0.42	0.98	0.42	0.98	0.58	0.42	0.98	0.42	0.98
600/750	0.35	0.16	0.64	0.31	0.63	0.38	0.29	0.76	0.38	0.83	0.38	0.3	0.76	0.38	0.83
600/850	0.32	0.21	0.62	0.45	0.68	0.41	0.29	0.73	0.48	0.84	0.41	0.29	0.73	0.48	0.84
600/1000	0.4	0.12	0.68	0.27	0.73	0.46	0.18	0.76	0.33	0.78	0.46	0.19	0.76	0.33	0.78
600/1200	0.44	0.21	0.61	0.26	0.72	0.49	0.28	0.71	0.33	0.8	0.49	0.28	0.72	0.33	0.8
625/750	0.33	0.17	0.62	0.22	0.75	0.37	0.28	0.73	0.27	0.79	0.37	0.29	0.73	0.27	0.79
650/800	0.27	0.1	0.57	0.22	0.63	0.32	0.2	0.67	0.26	0.73	0.32	0.2	0.67	0.26	0.73
650/850	0.28	0.1	0.75	0.37	0.84	0.33	0.17	0.75	0.4	0.84	0.33	0.17	0.75	0.4	0.84
700/705	0.48	0.37	0.84	0.42	0.89	0.5	0.52	0.88	0.45	0.91	0.5	0.52	0.88	0.45	0.91
700/720	0.39	0.26	0.72	0.64	0.77	0.55	0.4	0.82	0.7	0.88	0.55	0.4	0.82	0.7	0.88
800/805	0.22	0.27	0.62	0.23	0.58	0.28	0.48	0.68	0.35	0.8	0.28	0.48	0.68	0.35	0.8
800/850	0.25	0.19	0.58	0.33	0.61	0.27	0.26	0.64	0.34	0.68	0.27	0.26	0.64	0.34	0.68
800/1200	0.23	0.08	0.42	0.13	0.48	0.27	0.13	0.5	0.16	0.56	0.27	0.13	0.5	0.16	0.56

Table 3: Same as in Table 2 but for observed exclusions.

References

- [1] S. Coleman and J. Mandula, *All possible symmetries of the s matrix*, *Phys. Rev.* **159** (Jul, 1967) 1251–1256.
- [2] R. Haag, J. T. Lopuszanski, and M. Sohnius, *All Possible Generators of Supersymmetries of the s Matrix*, *Nucl. Phys. B* **88** (1975) 257.
- [3] J. Wess and B. Zumino, *Supergauge Transformations in Four-Dimensions*, *Nucl. Phys. B* **70** (1974) 39–50.
- [4] G. R. Farrar and P. Fayet, *Phenomenology of the Production, Decay, and Detection of New Hadronic States Associated with Supersymmetry*, *Phys. Lett. B* **76** (1978) 575–579.
- [5] G. Jungman, M. Kamionkowski, and K. Griest, *Supersymmetric dark matter*, *Phys. Rept.* **267** (1996) 195–373, [[hep-ph/9506380](#)].
- [6] **ATLAS** Collaboration, G. Aad et al., *Search for supersymmetry using final states with one lepton, jets, and missing transverse momentum with the ATLAS detector in $\sqrt{s} = 7$ TeV pp* , *Phys. Rev. Lett.* **106** (2011) 131802, [[arXiv:1102.2357](#)].
- [7] **CMS** Collaboration, V. Khachatryan et al., *Search for Supersymmetry in pp Collisions at 7 TeV in Events with Jets and Missing Transverse Energy*, *Phys. Lett. B* **698** (2011) 196–218, [[arXiv:1101.1628](#)].
- [8] **ATLAS** Collaboration, G. Aad et al., *Search for direct slepton and gaugino production in final states with two leptons and missing transverse momentum with the ATLAS detector in pp collisions at $\sqrt{s} = 7$ TeV*, *Phys. Lett. B* **718** (2013) 879–901, [[arXiv:1208.2884](#)].
- [9] **ATLAS** Collaboration, G. Aad et al., *Search for direct production of charginos and neutralinos in events with three leptons and missing transverse momentum in $\sqrt{s} = 8$ TeV pp collisions with the ATLAS detector*, *JHEP* **04** (2014) 169, [[arXiv:1402.7029](#)].
- [10] **CMS** Collaboration, S. Chatrchyan et al., *Search for electroweak production of charginos and neutralinos using leptonic final states in pp collisions at $\sqrt{s} = 7$ TeV*, *JHEP* **11** (2012) 147, [[arXiv:1209.6620](#)].
- [11] **CMS** Collaboration, *Search for direct EWK production of SUSY particles in multilepton modes with 8TeV data*, CMS-PAS-SUS-12-022.
- [12] **ATLAS** Collaboration, G. Aad et al., *Search for R -parity-violating supersymmetry in a final state containing leptons and many jets with the ATLAS experiment using $\sqrt{s} = 13$ TeV proton–proton collision data*, *Eur. Phys. J. C* **81** (2021), no. 11 1023, [[arXiv:2106.09609](#)].
- [13] **ATLAS** Collaboration, G. Aad et al., *Search for pair production of squarks or gluinos decaying via sleptons or weak bosons in final states with two same-sign or three leptons with the ATLAS detector*, *JHEP* **02** (2024) 107, [[arXiv:2307.01094](#)].
- [14] **ATLAS** Collaboration, G. Aad et al., *ATLAS Run 2 searches for electroweak production of supersymmetric particles interpreted within the p MSSM*, [[arXiv:2402.01392](#)].
- [15] **CMS** Collaboration, A. Hayrapetyan et al., *Search for new physics in multijet events with at least one photon and large missing transverse momentum in proton-proton collisions at 13 TeV*, *JHEP* **10** (2023) 046, [[arXiv:2307.16216](#)].
- [16] **CMS** Collaboration, A. Tumasyan et al., *Search for top squark pair production in a final state with at least one hadronically decaying tau lepton in proton-proton collisions at $\sqrt{s} = 13$ TeV*, *JHEP* **07** (2023) 110, [[arXiv:2304.07174](#)].

- [17] I. n. Lara, T. Buanes, R. Maselek, M. M. Nojiri, K. Rolbiecki, and K. Sakurai, *Monojet signatures from gluino and squark decays*, *JHEP* **10** (2022) 150, [[arXiv:2208.01651](#)].
- [18] **ATLAS** Collaboration, ATLAS Collaboration, *Reproducing searches for new physics with the ATLAS experiment through publication of full statistical likelihoods*, Tech. Rep. [ATL-PHYS-PUB-2019-029](#), 2019.
- [19] **CMS** Collaboration, CMS Collaboration, *Simplified likelihood for the re-interpretation of public CMS results*, Tech. Rep. [CMS-NOTE-2017-001](#), CERN, Geneva, Jan, 2017.
- [20] J. Y. Araz, A. Buckley, B. Fuks, H. Reyes-Gonzalez, W. Waltenberger, S. L. Williamson, and J. Yellen, *Strength in numbers: Optimal and scalable combination of LHC new-physics searches*, *SciPost Phys.* **14** (2023), no. 4 077, [[arXiv:2209.00025](#)].
- [21] M. M. Altakach, S. Kraml, A. Lessa, S. Narasimha, T. Pascal, T. Reymermier, and W. Waltenberger, *Global LHC constraints on electroweak-inos with SModelS v2.3*, [arXiv:2312.16635](#).
- [22] G. Alguero, J. Y. Araz, B. Fuks, and S. Kraml, *Signal region combination with full and simplified likelihoods in MadAnalysis 5*, *SciPost Phys.* **14** (2023), no. 1 009, [[arXiv:2206.14870](#)].
- [23] J. Alwall, R. Frederix, S. Frixione, V. Hirschi, F. Maltoni, O. Mattelaer, H. S. Shao, T. Stelzer, P. Torrielli, and M. Zaro, *The automated computation of tree-level and next-to-leading order differential cross sections, and their matching to parton shower simulations*, *JHEP* **07** (2014) 079, [[arXiv:1405.0301](#)].
- [24] L. Darmé et al., *UFO 2.0: the ‘Universal Feynman Output’ format*, *Eur. Phys. J. C* **83** (2023), no. 7 631, [[arXiv:2304.09883](#)].
- [25] C. Duhr and B. Fuks, *A superspace module for the FeynRules package*, *Comput. Phys. Commun.* **182** (2011) 2404–2426, [[arXiv:1102.4191](#)].
- [26] N. D. Christensen, P. de Aquino, C. Degrande, C. Duhr, B. Fuks, M. Herquet, F. Maltoni, and S. Schumann, *A Comprehensive approach to new physics simulations*, *Eur. Phys. J. C* **71** (2011) 1541, [[arXiv:0906.2474](#)].
- [27] A. Alloul, N. D. Christensen, C. Degrande, C. Duhr, and B. Fuks, *FeynRules 2.0 - A complete toolbox for tree-level phenomenology*, *Comput. Phys. Commun.* **185** (2014) 2250–2300, [[arXiv:1310.1921](#)].
- [28] S. Bailey, T. Cridge, L. A. Harland-Lang, A. D. Martin, and R. S. Thorne, *Parton distributions from LHC, HERA, Tevatron and fixed target data: MSHT20 PDFs*, *Eur. Phys. J. C* **81** (2021), no. 4 341, [[arXiv:2012.04684](#)].
- [29] A. Buckley, J. Ferrando, S. Lloyd, K. Nordström, B. Page, M. Rüfenacht, M. Schönherr, and G. Watt, *LHAPDF6: parton density access in the LHC precision era*, *Eur. Phys. J. C* **75** (2015) 132, [[arXiv:1412.7420](#)].
- [30] J. Fiaschi, B. Fuks, M. Klasen, and A. Neuwirth, *Electroweak superpartner production at 13.6 Tev with Resummino*, *Eur. Phys. J. C* **83** (2023), no. 8 707, [[arXiv:2304.11915](#)].
- [31] W. Beenakker, C. Borschensky, M. Krämer, A. Kulesza, and E. Laenen, *NNLL-fast: predictions for coloured supersymmetric particle production at the LHC with threshold and Coulomb resummation*, *JHEP* **12** (2016) 133, [[arXiv:1607.07741](#)].
- [32] A. P. Neuwirth, *Apn-pucky/hepi: Zenodo release*, Oct., 2023.

- [33] G. F. Sterman, *Summation of Large Corrections to Short Distance Hadronic Cross-Sections*, *Nucl. Phys. B* **281** (1987) 310–364.
- [34] S. Catani and L. Trentadue, *Resummation of the QCD Perturbative Series for Hard Processes*, *Nucl. Phys. B* **327** (1989) 323–352.
- [35] A. Vogt, *Next-to-next-to-leading logarithmic threshold resummation for deep inelastic scattering and the Drell-Yan process*, *Phys. Lett. B* **497** (2001) 228–234, [[hep-ph/0010146](#)].
- [36] W. Beenakker, M. Klasen, M. Kramer, T. Plehn, M. Spira, and P. M. Zerwas, *The Production of charginos / neutralinos and sleptons at hadron colliders*, *Phys. Rev. Lett.* **83** (1999) 3780–3783, [[hep-ph/9906298](#)]. [Erratum: *Phys.Rev.Lett.* 100, 029901 (2008)].
- [37] J. Fiaschi and M. Klasen, *Higgsino and gaugino pair production at the LHC with $a\text{NNLO}+\text{NNLL}$ precision*, *Phys. Rev. D* **102** (2020), no. 9 095021, [[arXiv:2006.02294](#)].
- [38] J. Debove, B. Fuks, and M. Klasen, *Threshold resummation for gaugino pair production at hadron colliders*, *Nucl. Phys. B* **842** (2011) 51–85, [[arXiv:1005.2909](#)].
- [39] B. Fuks, M. Klasen, D. R. Lamprea, and M. Rothering, *Gaugino production in proton-proton collisions at a center-of-mass energy of 8 TeV*, *JHEP* **10** (2012) 081, [[arXiv:1207.2159](#)].
- [40] J. Fiaschi and M. Klasen, *Neutralino-chargino pair production at $\text{NLO}+\text{NLL}$ with resummation-improved parton density functions for LHC Run II*, *Phys. Rev. D* **98** (2018), no. 5 055014, [[arXiv:1805.11322](#)].
- [41] J. Baglio, G. Coniglio, B. Jager, and M. Spira, *Next-to-leading-order QCD corrections and parton-shower effects for weakino+squark production at the LHC*, *JHEP* **12** (2021) 020, [[arXiv:2110.04211](#)].
- [42] J. Fiaschi, B. Fuks, M. Klasen, and A. Neuwirth, *Soft gluon resummation for associated squark-electroweakino production at the LHC*, *JHEP* **06** (2022) 130, [[arXiv:2202.13416](#)].
- [43] W. Beenakker, R. Hopker, M. Spira, and P. M. Zerwas, *Squark and gluino production at hadron colliders*, *Nucl. Phys. B* **492** (1997) 51–103, [[hep-ph/9610490](#)].
- [44] U. Langenfeld and S.-O. Moch, *Higher-order soft corrections to squark hadro-production*, *Phys. Lett. B* **675** (2009) 210–221, [[arXiv:0901.0802](#)].
- [45] A. Kulesza and L. Motyka, *Threshold resummation for squark-antisquark and gluino-pair production at the LHC*, *Phys. Rev. Lett.* **102** (2009) 111802, [[arXiv:0807.2405](#)].
- [46] A. Kulesza and L. Motyka, *Soft gluon resummation for the production of gluino-gluino and squark-antisquark pairs at the LHC*, *Phys. Rev. D* **80** (2009) 095004, [[arXiv:0905.4749](#)].
- [47] W. Beenakker, S. Brensing, M. Kramer, A. Kulesza, E. Laenen, and I. Niessen, *Soft-gluon resummation for squark and gluino hadroproduction*, *JHEP* **12** (2009) 041, [[arXiv:0909.4418](#)].
- [48] W. Beenakker, S. Brensing, M. Kramer, A. Kulesza, E. Laenen, and I. Niessen, *NNLL resummation for squark-antisquark pair production at the LHC*, *JHEP* **01** (2012) 076, [[arXiv:1110.2446](#)].
- [49] W. Beenakker, T. Janssen, S. Lepoeter, M. Krämer, A. Kulesza, E. Laenen, I. Niessen, S. Thewes, and T. Van Daal, *Towards NNLL resummation: hard matching coefficients for squark and gluino hadroproduction*, *JHEP* **10** (2013) 120, [[arXiv:1304.6354](#)].
- [50] W. Beenakker, C. Borschensky, M. Krämer, A. Kulesza, E. Laenen, V. Theeuwes, and

- S. Thewes, *NNLL resummation for squark and gluino production at the LHC*, *JHEP* **12** (2014) 023, [[arXiv:1404.3134](#)].
- [51] W. Beenakker, C. Borschensky, M. Krämer, A. Kulesza, E. Laenen, S. Marzani, and J. Rojo, *NLO+NLL squark and gluino production cross-sections with threshold-improved parton distributions*, *Eur. Phys. J. C* **76** (2016), no. 2 53, [[arXiv:1510.00375](#)].
- [52] W. Beenakker, R. Hopker, and M. Spira, *PROSPINO: A Program for the production of supersymmetric particles in next-to-leading order QCD*, [hep-ph/9611232](#).
- [53] G.-p. Gao, G.-r. Lu, Z.-h. Xiong, and J. M. Yang, *Loop effects and nondecoupling property of SUSY QCD in $g b \rightarrow t H^-$* , *Phys. Rev. D* **66** (2002) 015007, [[hep-ph/0202016](#)].
- [54] C. Bierlich et al., *A comprehensive guide to the physics and usage of PYTHIA 8.3*, *SciPost Phys. Codeb.* **2022** (2022) 8, [[arXiv:2203.11601](#)].
- [55] S. Catani, F. Krauss, R. Kuhn, and B. R. Webber, *QCD matrix elements + parton showers*, *JHEP* **11** (2001) 063, [[hep-ph/0109231](#)].
- [56] L. Lonnblad, *Correcting the color dipole cascade model with fixed order matrix elements*, *JHEP* **05** (2002) 046, [[hep-ph/0112284](#)].
- [57] L. Lonnblad and S. Prestel, *Matching Tree-Level Matrix Elements with Interleaved Showers*, *JHEP* **03** (2012) 019, [[arXiv:1109.4829](#)].
- [58] E. Conte, B. Fuks, and G. Serret, *MadAnalysis 5, A User-Friendly Framework for Collider Phenomenology*, *Comput. Phys. Commun.* **184** (2013) 222–256, [[arXiv:1206.1599](#)].
- [59] E. Conte, B. Dumont, B. Fuks, and C. Wymant, *Designing and recasting LHC analyses with MadAnalysis 5*, *Eur. Phys. J. C* **74** (2014), no. 10 3103, [[arXiv:1405.3982](#)].
- [60] E. Conte and B. Fuks, *Confronting new physics theories to LHC data with MADANALYSIS 5*, *Int. J. Mod. Phys. A* **33** (2018), no. 28 1830027, [[arXiv:1808.00480](#)].
- [61] **DELPHES 3** Collaboration, J. de Favereau, C. Delaere, P. Demin, A. Giammanco, V. Lemaître, A. Mertens, and M. Selvaggi, *DELPHES 3, A modular framework for fast simulation of a generic collider experiment*, *JHEP* **02** (2014) 057, [[arXiv:1307.6346](#)].
- [62] J. Y. Araz, B. Fuks, and G. Polykratis, *Simplified fast detector simulation in MADANALYSIS 5*, *Eur. Phys. J. C* **81** (2021), no. 4 329, [[arXiv:2006.09387](#)].
- [63] J. Y. Araz, *Spey: smooth inference for reinterpretation studies*, *SciPost Phys.* **16** (2024) 032, [[arXiv:2307.06996](#)].
- [64] **ATLAS** Collaboration, G. Aad et al., *Search for new phenomena in events with an energetic jet and missing transverse momentum in pp collisions at $\sqrt{s} = 13$ TeV with the ATLAS detector*, *Phys. Rev. D* **103** (2021), no. 11 112006, [[arXiv:2102.10874](#)].
- [65] **ATLAS** Collaboration, G. Aad et al., *Search for squarks and gluinos in final states with jets and missing transverse momentum using 139 fb^{-1} of $\sqrt{s} = 13$ TeV pp collision data with the ATLAS detector*, *JHEP* **02** (2021) 143, [[arXiv:2010.14293](#)].
- [66] **CMS** Collaboration, T. C. Collaboration et al., *Search for supersymmetry in proton-proton collisions at 13 TeV in final states with jets and missing transverse momentum*, *JHEP* **10** (2019) 244, [[arXiv:1908.04722](#)].
- [67] **CMS** Collaboration, A. Tumasyan et al., *Search for new particles in events with energetic jets and large missing transverse momentum in proton-proton collisions at $\sqrt{s} = 13$ TeV*, *JHEP* **11** (2021) 153, [[arXiv:2107.13021](#)].

- [68] F. Ambrogio, *Implementation of a search for squarks and gluinos in the multi-jet + missing energy channel (139 fb⁻¹; 13 TeV; ATLAS-CONF-2019-040)*, doi:10.14428/DVN/NW3NPG.
- [69] D. Agin, *Implementation of a search for new physics with jets and missing transverse energy (139/fb; 13 TeV; ATLAS-EXOT-2018-06)*, doi:10.14428/DVN/REPAMM.
- [70] M. Malte, S. Bein, and J. Sonneveld, *Re-implementation of a search for supersymmetry in the HT/missing HT channel (137 fb⁻¹; CMS-SUSY-19-006)*, doi:10.14428/DVN/4DEJQM.
- [71] A. Albert, *Implementation of a search for new phenomena in events featuring energetic jets and missing transverse energy (137 fb⁻¹; 13 TeV; CMS-EXO-20-004)*, doi:10.14428/DVN/IRF7ZL.
- [72] B. Dumont, B. Fuks, S. Kraml, S. Bein, G. Chalons, E. Conte, S. Kulkarni, D. Sengupta, and C. Wymant, *Toward a public analysis database for LHC new physics searches using MADANALYSIS 5*, *Eur. Phys. J. C* **75** (2015), no. 2 56, [[arXiv:1407.3278](#)].
- [73] J. Y. Araz, M. Frank, and B. Fuks, *Reinterpreting the results of the LHC with MadAnalysis 5: uncertainties and higher-luminosity estimates*, *Eur. Phys. J. C* **80** (2020), no. 6 531, [[arXiv:1910.11418](#)].
- [74] J. Kim, T. Lee, J. Kim, and H. Jang, *Implementation of the ATLAS-SUSY-2018-06 analysis in the MadAnalysis 5 framework (electroweakinos with Jigsaw variables; 139 fb⁻¹)*, *Mod. Phys. Lett. A* **36** (2021), no. 01 2141004.
- [75] M. Mrowietz, S. Bein, and J. Sonneveld, *Implementation of the CMS-SUS-19-006 analysis in the MadAnalysis 5 framework (supersymmetry with large hadronic activity and missing transverse energy; 137 fb⁻¹)*, *Mod. Phys. Lett. A* **36** (2021), no. 01 2141007.
- [76] B. Fuks et al., *Proceedings of the second MadAnalysis 5 workshop on LHC recasting in Korea*, *Mod. Phys. Lett. A* **36** (2021), no. 01 2102001, [[arXiv:2101.02245](#)].
- [77] G. Cowan, K. Cranmer, E. Gross, and O. Vitells, *Asymptotic formulae for likelihood-based tests of new physics*, *Eur. Phys. J. C* **71** (2011) 1554, [[arXiv:1007.1727](#)]. [Erratum: *Eur.Phys.J.C* 73, 2501 (2013)].